MR Directed Focal Hyperthermia for Pelvic Disease

Mid-Term Progress Report

September 5, 2013

PI - Chris J Diederich, PhD

AIM 1 Implement operational modifications and integrate custom multi-slice or volumetric MR temperature guidance and system control as required to utilize the InSightec 2100 ER array to deliver targeted and long-duration continuous hyperthermia (versus pulsed hyperthermia).

We have worked closely with Insightec to establish the existing system constraints (imposed by original design for producing and monitoring short, tightly focused sonications specific to ablation) and devised communication protocols to control the Insightec Prostate phased array through the CPC interface. During our interactions we were able to work with the engineers to determine some parameters such as maximum allowable power levels and duration of CW application, and have now applied these values to our control algorithms. In this fashion, we can modify the applied surface intensity, individual or customized complex phase patterns, sequence duration, position regeneration, phasing patterns, and other applicator parameters – as demonstrated to allow protracted or long duration hyperthermia over a large contiguous volume. Custom multi-slice MRTI using RTHawk was developed for this application and implemented to monitor the hyperthermia temperature elevations over the loner intervals required. (See attached SPIE publication and submitted manuscript).

Next steps: include streamlining control with a GUI specific to this application, which can implement the phasing patterns and control techniques from Aim 2 studies. RTHawk multi-slice MRTI will be modified to measure defined temperature ROI's and be used to apply feedback control of applied power.

AIM 2 Design and evaluate treatment delivery strategies using patient-specific simulations.

3D patient specific models were created, selected to bracket anticipated clinical treatment sites. MR images that clearly delineate focal disease were obtained and used to generate 3D biothermal models, together with complex acoustic field calculations within the prostate and defined intraprostatic lesions. The acoustic simulations were specific to the Insightec array layout and wiring (this information was given to us on a confidential and proprietary basis). Determination and assessment of various phasing patterns for generating conformal and effective hyperthermia for various locations and dimensions of tumor target were performed. General phasing patterns, with either multipoint single focus, diverging, converging, and planar static patterns were investigated, as well multi-point electronic scanning, and clearly demonstrated feasibility of this approach and potential for implementation in human studies. (See attached SPIE publication and submitted manuscript for details).

Next steps: include investigation of temperature-based feedback control schemes for real-time modulation of phased array sonications. Placing temperature ROI's from RTHawk MRTI measurements in control loops, to vary applied surface intensity.

AIM 3 Validate and characterize system performance within tissue phantoms and in vivo models. The modified ER ablation system and preliminary controlling software, along with calculated phasing patterns (from Aim 2) for a variety of tumor shapes and target localization were evaluated in static tissue mimicking phantom within the MR using RTHawk to setup and monitor temperature. These experiments demonstrated hyperthermia delivery can be performed, albeit in a non-perfused environment. Key points demonstrated that there is very little ripple in the temperature distributions achieved accounting for hardware limitations, and that total acoustic power output is not limited and appears to be sufficient. (See attached SPIE publication and submitted manuscript for more details).

Next steps: we plan to generate more complex beam patterns and implement control feedback algorithms, and evaluate in phantoms and ex vivo tissues. We will also investigate approaches to use the internal mechanical positioning of the Insightec system for real-time mechanical scanning, at least in the discrete versus continuous movement setting, and we will use multi-baseline MRTI with RTHawk. Finally, we will evaluate in animal studies as proposed, following our currently approved protocol (see attached Approval Letter - AN088193-01 - MR-guided cardiac focused ultrasound ablation – PI, Viola Rieke), as amended to include endorectal heating and targeting thigh muscle, as we proposed, in addition to cardiac studies. Specifically, the complex acoustic waveforms, MRTI, and feedback control will be validated and performance characterized to define the Insightec capabilities to generate and control ultrasound intensity distributions and hyperthermia delivery in vivo within porcine perfused tissue models. These are critical performance indexes to track this technology quickly into clinical implementation.

Administrative Notes: we required considerable ramp-up time due to unforeseen closure of the MR suite (the shield room ceiling fell in, and reconstruction was required). We are requesting a no-cost extension to extend this effort for four additional months, to end March 31, 2014 instead of November 2013.

Publications (also attached)

- *Salgaonkar VA*, Prakash P, Rieke V, Ozhinsky E, Plata J, Kurhanewicz J, Hsu IC, Diederich CJ. Model-based feasibility assessment and evaluation of prostate hyperthermia with a commercial MR-guided endorectal HIFU ablation array. Medical Physics [under review].

- *Salgaonkar VA*, Prakash P, Plata J, Holbrook A, Rieke V, Kurhanewicz J, Hsu I-C, Diederich CJ. Targeted hyperthermia in prostate with an MR-guided endorectal ultrasound phased array: patient specific modeling and preliminary experiments. Proc SPIE 8584 2013.

Abstracts/Oral Presentations

- Salgaonkar VA, Rieke V , Ozhinsky E, Prakash P, Plata J, Kurhanewicz J, Hsu IC, Diederich CJ. Model-based Feasibility Assessment and Evaluation of Prostate Hyperthermia with a Commercial MR-guided Endorectal HIFU Ablation Array. Annual Meeting Acoustical Society of America, San Francisco, CA, USA Dec. 2013

- Salgaonkar VA, Rieke V , Ozhinsky E, Prakash P, Kurhanewicz J, Hsu IC, Diederich CJ. Model-based feasibility assessment and evaluation of prostate hyperthermia with a commercial MR-guided endorectal HIFU ablation array. 2nd European Symposium on Focused Ultrasound Therapy. Rome, Italy,. Oct. 2013
- Salgaonkar VA, Rieke V , Chang A, Hsu IC, Kurhanewicz J, Scott S, Plata J, Diederich CJ. MR-guided endocavity ultrasound hyperthermia for treating pelvic malignancies: patient specific modelling and preliminary experiments. Annual Symposium Society for Thermal Medicine. Aruba, Apr. 2013.
- Salgaonkar VA, Prakash P, Plata J, Holbrook A, Rieke V, Kurhanewicz J, Hsu IC, Diederich CJ. Targeted hyperthermia in prostate with an MR-guided endorectal ultrasound phased array: patient specific modeling and preliminary experiments. Photonics West Symposium, SPIE, San Francisco CA, USA, Jan. 2013.

Targeted hyperthermia in prostate with an MR-guided endorectal ultrasound phased array: patient specific modeling and preliminary experiments

Vasant A. Salgaonkar[1], Punit Prakash[1], Juan Plata[2], Andrew Holbrook[2] Viola Rieke[3], John Kurhanewicz[3], I-C (Joe) Hsu[1], Chris J. Diederich[1]
[1]Radiation Oncology, University of California San Francisco
1600 Divisadero St. Suite H-1031, San Francisco, CA USA 94143
[2]Radiology, Stanford University
1201 Welch Rd. Stanford CA USA 94305
[3]Radiology and Biomedical Imaging, University of California San Francisco
505 Parnassus Ave., San Francisco CA USA 94143

ABSTRACT

Feasibility of hyperthermia delivery to the prostate with a commercially available MR-guided endorectal ultrasound (ERUS) phased array ablation system (ExAblate 2100, Insightec, LTD) was assessed through computer simulations and *ex vivo* experiments.

The simulations included a 3D FEM-based biothermal model, and acoustic field calculations for the ExAblate phased array (2.3 MHz, 2.3×4.0 cm^2) using the rectangular radiator method. Array beamforming strategies were investigated to deliver 30-min hyperthermia (>41 ^oC) to focal regions of prostate cancer, identified from MR images in representative patient cases. Constraints on power densities, sonication durations and switching speeds imposed by ExAblate hardware and software were incorporated in the models. T>41 ^oC was calculated in 14–19 cm^3 for sonications with planar or diverging beam patterns at 0.9–1.2 W/cm^2, and in 3-10 cm^3 for curvilinear (cylindrical) or multifocus beam patterns at 1.5–3.3 W/cm^2, potentially useful for treating focal disease in a single posterior quadrant.

Preliminary experiments included beamformed sonications in tissue mimicking phantom material under MRI-based temperature monitoring at 3T (GRE TE=7.0 ms, TR=15 ms, BW=10.5 kHz, FOV=15 cm, matrix 128x128, FA=40º). MR-temperature rises of 2-6 ^oC were induced in a phantom with the ExAblate array, consistent with calculated values and lower power settings (~0.86 W/cm^2, 3 min.).

Conformable hyperthermia may be delivered by tailoring power deposition along the array length and angular expanse. MRgERUS HIFU systems can be controlled for continuous hyperthermia in prostate to augment radiotherapy and drug delivery. [FUS Foundation, NIH R01 122276, 111981].

Keywords: hyperthermia, MR-guided HIFU, endorectal ultrasound, phased array, beamforming, modeling, simulation.

1. INTRODUCTION

Hyperthermia has been combined successfully with radiation therapy and chemotherapy to improve cancer treatment outcomes.[1, 2] For maximum clinical benefit, uniform temperature profiles are desired within target volumes for 30 – 60 min duration, with minimum temperature greater than 40 ^oC and 6 – 10 min cumulative thermal dose at 43 ^oC.[3-5] Administering hyperthermia to tumors situated deep inside the body presents significant clinical challenges such as, selective energy deposition within the tumor while thermally sparing surrounding structures, and sufficient thermometry for reliable treatment monitoring.[6] These difficulties are also associated with hyperthermia delivery to focal tumors in prostate and other organs inside the pelvic cavity.

Hyperthermia applicators based on ultrasound energy have been under development because they enable spatially controlled energy deposition and selective tumor heating. Devices designed for prostate hyperthermia include interstitial linear array applicators with tubular ultrasound transducers[5, 7] and endorectal ultrasound (ERUS) phased arrays[8-10] used in combination with radiation therapy. Currently, MR guided high intensity focused ultrasound (HIFU) systems are being increasingly utilized for noninvasive or minimally-invasive thermal ablation of soft tissue tumors in multiple organ

Energy-based Treatment of Tissue and Assessment VII, edited by Thomas P. Ryan, Proc. of SPIE
Vol. 8584, 85840U · © 2013 SPIE · CCC code: 1605-7422/13/$18 · doi: 10.1117/12.2004609

sites.[11] Typically, these are multi-element phased array applicators capable of delivering ultrasound energy with precise spatial control. Combined with MR-based thermometry, such HIFU ablation procedures can be monitored and guided in real time. Endorectal ultrasound applicators, consisting of phased arrays or multi-sectored devices, have been investigated for delivering hyperthermia under MR guidance and control.[8, 9] Recent animal studies have utilized commercial MR-guided HIFU systems for enhancement of drug delivery This has been achieved through pulsed-mode operation of the HIFU system for enhancement of uptake of free flowing drug[12] or rapid electro-mechanical translation of the HIFU focus to heat small volumes and deliver drugs encapsulated in temperature sensitive liposomes.[13]

ExAblate 2100 (InSigtec LTD) is a commercially available MR-guided ablation system. It consists of an ERUS phased array designed for prostate ablation (Figure 1) and software platform for treatment planning and monitoring. In contrast to HIFU which utilizes highly-focused, high-power and short-duration sonications, hyperthermia requires diffused energy deposition to establish uniform temperature distribution in the entire tumor volume over a long time interval. Hence, in this study, feasibility of protracted (as opposed to pulsed) hyperthermia to large prostate targets (focal tumors, posterior quadrants, hemi-gland) with the ExAblate array was assessed through simulations, modeling and preliminary experiments. Operational modifications required for continuous wave (CW) mode sonications and continuous volumetric multi-plane MRTI were identified within system hardware and software constraints. The ExAblate system is already in clinical trials for prostate ablation. If it can be successfully adapted for mild hyperthermia, it can be potentially fast-tracked for clinical application. With this motivation, the initial study presented here was planned to identify operational modifications, feasibility and capability of safe and reliable MR-guided prostate hyperthermia with ExAblate 2100.

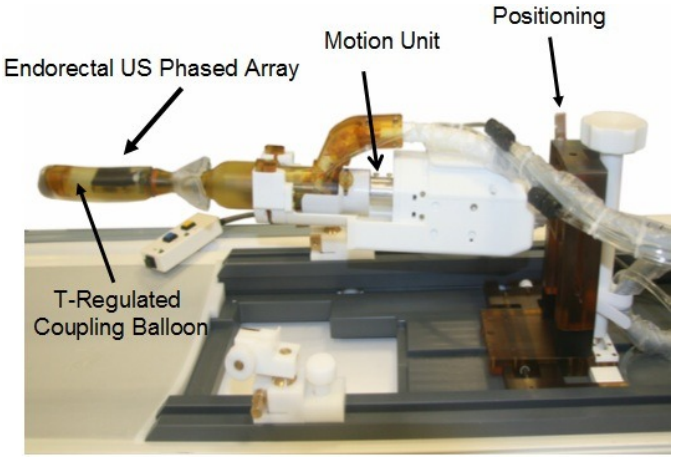

Figure 1: Photograph of ExAblate 2100 endorectal phased array prostate ablation system is shown. Positioning and motion units are useful for array placement, rotation and translation. The device is coupled to the rectal wall using a latex balloon containing temperature regulated water for transducer cooling and rectal wall protection.

2. SIMULATIONS

2.1 Acoustic models

Acoustic pressure field distributions generated by ExAblate 2100 phased array were simulated using the rectangular radiator method.[14] Specifications of ExAblate 2100 such as operating frequency (2.3 MHz), array dimensions (23×40 mm^2), independent power channels (~990), proprietary element size, element layout and electrical connections, proprietary hardware switching speeds and power limitations were incorporated in the acoustic models. For a planar phased array in plane $z = 0$, the mathematical expression for acoustic pressure was written as

$$p_0(x,y,z) = \frac{j\rho c \Delta A}{\lambda} \sum_{n=1}^{N} \frac{u_n}{R} e^{-jkR} \sin c\left[\frac{k(x-x_n)\Delta w}{2R}\right] \sin c\left[\frac{k(y-y_n)\Delta h}{2R}\right]. \quad (1)$$

In Eq. 1, ρ is density, c is speed of sound, λ is wavelength, k is wave-number, $u_n = |u_n| \times \exp(-j\varphi_n)$ is complex particle velocity at the surface of the n^{th} element and φ_n is phase, Δw, Δh, ΔA are width, height and surface area of an element

respectively , x_n and y_n are centers of the n^{th} element, and $R = [z^2 + (x\text{-}x_n)^2 + (y\text{-}y_n)^2]^{0.5}$. Throughout this paper, x, y and z dimensions of the array have been referred to as azimuth, elevation, and axial depth or range, respectively. When computing the absorbed ultrasound energy (Q_{ac}), acoustic attenuation changes only in the axial or Z-directions were included and de-phasing or defocusing due to tissue non-homogeneity was not included in the models. Reflection, refraction or scattering phenomena at soft tissue – water and soft tissue – bone interfaces were also not included in the models. 100% transmission of longitudinal acoustic waves was assumed at the bone-tissue interface.

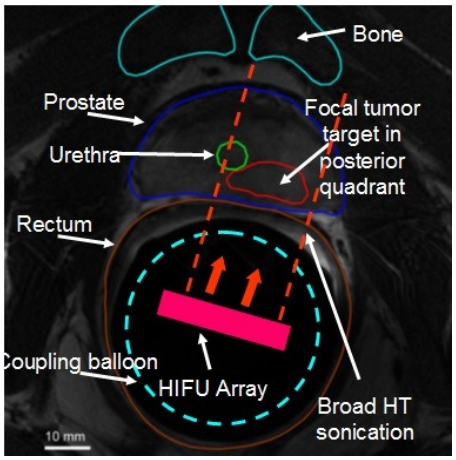

Figure 2: An example of patient-specific model geometry is shown with critical anatomical structures segmented on MRI in axial plane.

2.2 Biothermal models

During clinical hyperthermia procedures, it is desired that the temperature distributions be held steady above 41 °C within a given target volume. Such a situation can be modeled using the steady-state version of Pennes bioheat transfer equation.[15] Mathematically, this can be expressed as

$$\nabla[k \cdot \nabla\ T(x,y,z)] - \omega_b \cdot C_b \cdot [T(x,y,z) - T_b] + Q_{ac}(x,y,z) = 0. \quad (2)$$

In Eq. 3, T is tissue temperature, k is thermal conductivity, ω_b is blood perfusion, C_b is specific heat of blood, T_b is blood temperature, and ∇ operator refers to partial derivative in space.

This model was tested on generalized and patient-specific models. The generalized model geometry consisted of the ERUS phased array situated inside a 15-mm radius cylindrical latex balloon (acoustically transparent) sonicating a homogenous soft tissue with constant blood perfusion, acoustic parameters and thermal properties. Patient-specific models were created from MRI axial scans of representative patient cases. Anatomical structures in the pelvic cavity, such as prostate, hyperthermia target volume, rectum, bladder, urethra and pubic bones, were manually segmented using a commercially available radiation treatment planning software program (Oncentra, Nucleotron, Netherlands). All soft tissues were assumed to have identical acoustic and thermal properties, and blood perfusion. Bone was assumed to have higher acoustic attenuation and absorption, and no blood perfusion. The ERUS array (within a cylindrical balloon) was positioned such that the prostate would be centered over its length (40-mm dimension), and it was oriented to direct US energy towards a defined target volume (Figure 2).

Finite element methods (FEM) were employed to evaluate Eq. 2 using COMSOL Multiphysics (Comsol Inc., Palo Alto, CA, USA). To obtain a stable temperature solution, mesh size was restricted to 1.0 mm at the applicator-rectum interface, bone-soft-tissue interface, and in the region of maximum heating Dirichlet boundary conditions were set at constant body/basal temperature (37 °C) at the extremities of the simulation domain and constant cooling water temperature (30 - 35 °C) at the applicator-rectum boundary. Values of all constants and material parameters can be found in Table 1.

Table 1: List of parameters used in acoustic and biothermal models[16-18]

Parameter	Units	Value
k (thermal conductivity)	W/m/^{o}C	0.56
ω_b (blood perfusion)	kg/m^3/s	2.0 (soft-tissue) 0 (bone)
C_b (specific heat of blood)	J/kg/^{o}C	3720
T_b (body/blood temperature)	^{o}C	37
c (sound speed)	m/s	1500
ρ (density)	Kg/m^3	1060
f_0 (center frequency)	MHz	2.3
α (absorption coefficient)	Np/m/MHz	5.3 (soft tissue) 250 (bone)
μ (attenuation coefficient)	Np/m/MHz	5.3 (soft tissue) 250 (bone)

2.3 Hyperthermia-specific beamforming and sonications

Phase delays were computed for ERUS array channels based on array dimensions and layout. Beamforming techniques were employed and several sonication patterns, as shown below, were simulated.

Multi-point focusing: To selectively heat small targets, beamforming techniques which simultaneously focus the ERUS array at multiple (4 - 8) points were explored. An example of such targeting is shown in Figure 3a where hyperthermia to a small focal tumor in right posterior quadrant of the prostate was simulated. Focal point placement was ascertained through a manual iterative process to maximize target coverage, and the ERUS array was simultaneously focused on 6 points such that the resultant heating best conformed to the tumor shape. In the example shown here, acoustic intensity was 2.4 W/cm^2 (electrical power ~ 25 W) and maximum temperature was 44.2 ^{o}C. Calculated 41 ^{o}C contour covered the target volume.

Cylindrical or curvilinear focusing To simulate focusing behavior of a curvilinear or cylindrically focused transducer, the ERUS array was focused at constant depth along the entire array length in the elevation direction. Phase delays were computed based on the distance between ERUS elements and a cylindrical focus axis. This sonication pattern allowed heating in wedge-shaped patterns. For the representative case shown here, only elements in the central 2/3rd elevation span of the array were excited. The input was set to 0.7 W/cm^2 (electrical power ~ 8 W) and maximum temperature was 45 ^{o}C (Figure 3b).

Planar sonications: Planar beam patterns were simulated by setting uniform phase values for all power channels (Figure 3c). This achieved the effect of synchronous operation of all ERUS array elements to mimic the functionality of a planar rectangular transducer with a large aperture. Diffused energy deposition enabled treatment of large targets in the posterior quadrant of the prostate or hemi-gland prostate. Large volumes could be heated at relatively low power (~4 W) with low maximum temperature values (42.5 ^{o}C).

Diverging sonications: Diverging acoustic beam patterns were simulated to heat wide targets in posterior prostate (Figure 3d). Patient specific models were used to explore the possibility of heating bilateral targets with this configuration. To heat representative target shown in Figure 3d, the synthetic focus was placed 10 mm behind the array along the entire array elevation. This resulted in wave fronts similar to tubular transducer elements (cylindrically diverging or defocused). For the case shown here, urethra was close to the target and hence maximum temperature of 43.2 ^{o}C was calculated near the urethra. Some bone heating was also calculated (maximum = 41.5 ^{o}C).

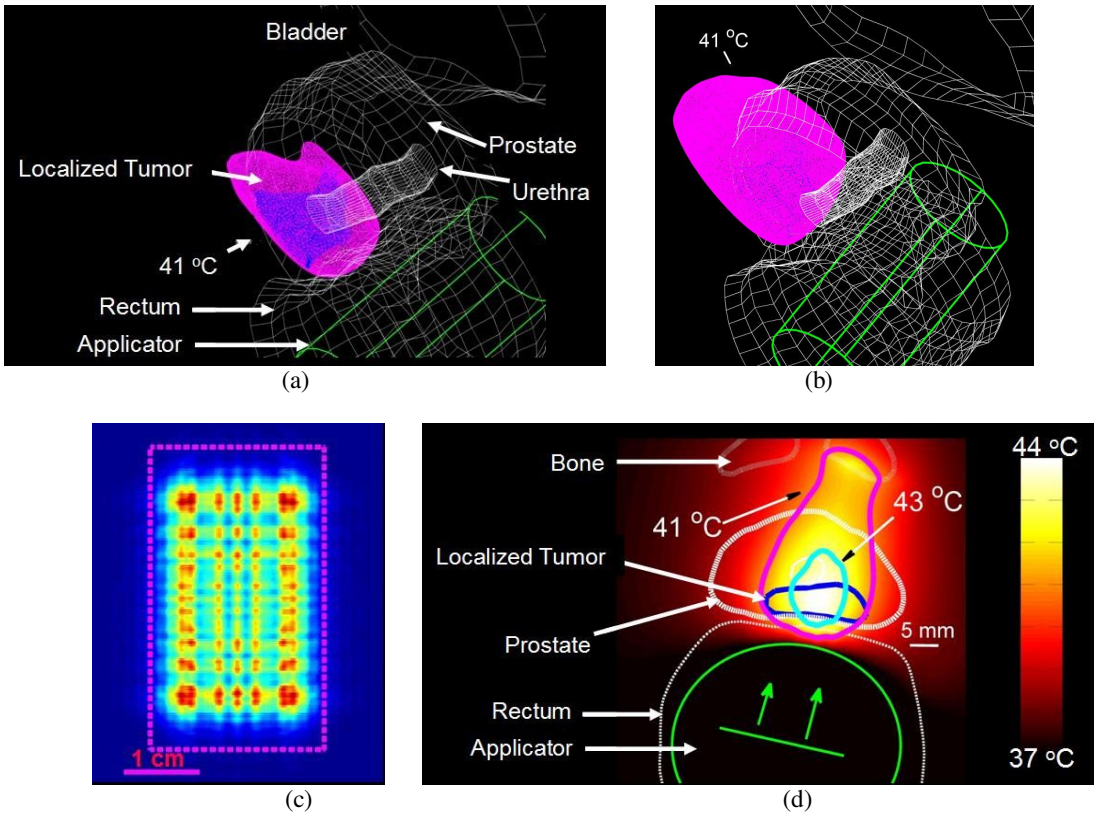

Figure 3**:** (a) In this model, a multi-focus pattern was employed to treat localized tumor in posterior prostate with acoustic input intensity was 2.4 W/cm^2 (~25 W electrical power) and maximum temperature was 44.2 ^{o}C. (b) Here, a cylindrical or curvilinear focus pattern was employed for hyperthermia delivery. Acoustic input intensity was 0.7 W/cm^2 (~8 W electrical power) and maximum temperature was 45.0 ^{o}C. (c) Normalized acoustic intensity in a coronal plane because of planar or uniform-phase sonication is shown at axial depth = 40 mm. Relative position of the transducer is shown by dotted rectangle. (d) Temperature distribution from a model of hyperthermia with diverging sonication demonstrates bilateral tumor targeting.

Generalized models were used to estimate treatment volume coverage and limits on the shapes of beamformed sonication patterns. Large treatment volumes could be heated with planar and diverging configurations. For input power of 10 – 14 W (0.9 – 1.2 W/cm^2), 41 ^{o}C iso-temperature volumes of 14 - 19 cm^3 and 40 ^{o}C iso-temperature volumes of 26 – 30 cm^3 could be established with maximum temperature between 43.5 – 44.7 ^{o}C. For divergence angles below 60^o, energy deposition in the side lobes did not cause excessive heating. With multi-focus sonications, relatively small volumes 3 – 6 cm^3 could be heated to T>41 ^{o}C. This required high input power of 40 W (~3.5 W/cm^2) and also resulted in maximum temperatures between 45 – 46 ^{o}C in small volumes. Steering angles greater than 15^o resulted in energy deposition in the side lobes (>15%). With curvilinear focusing, 10 cm^3 volumes could be heated above 41 ^{o}C with input power of 18 W (1.5 W/cm^2) and maximum temperature of 45 ^{o}C. Shallow focusing (<20 mm) and wide steering angles (>15^o) resulted in heating in the side lobes.

3. PRELIMINARY EXPERIMENTS

Preliminary experiments were conducted in tissue mimicking phantom material. The phantom was sonicated using ExAblate 2100 ERUS ablation array. Array beamforming schemes identified in the simulation study were programmed in the ExAblate system using the built-in CPC computer interface. Continuous-wave (CW) sonications at 0.86 W/cm^2 were applied for 3 minute durations. The experiment was conducted in a 3T MRI scanner (GE Healthcare MR750) and

MR images were acquired using two 5-inch surface imaging coils (schematic shown in Figure 4a). The MR images were recorded with sequences optimized for MR temperature monitoring (echo time = 7 ms, field-of-view = 15 cm, and image size = 128×128 pixels). MR thermometry was performed in real time using RTHawk (HeartVista Inc, Palo Alto, CA), a commercially available software platform which enabled real time access to the MR scanner settings and parameters, volumetric multi-plane imaging and dynamic image plane positioning, and fast temperature reconstruction from the MR images.

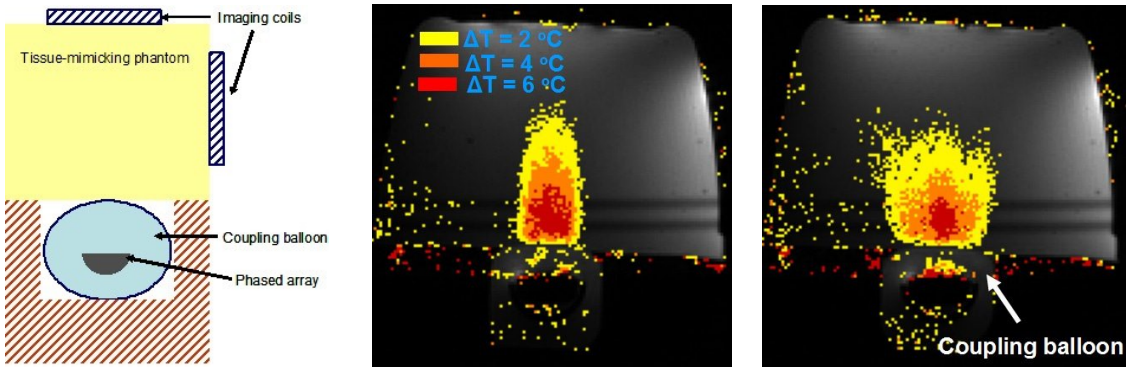

(a) (b) (c)

Figure 4: (a) ExAblate 2100 was operated to deliver hyperthermia and tested in a phantom model under MR temperature monitoring and a schematic diagram of the experiment set up is shown. Example MR temperature images (axial) captured during CW sonications in tissue mimicking phantoms with ExAblate 2100 array are shown here (0.86 W/cm^2, 3 min.). Heating from (b) electronically scanned sonications and (c) diverging sonications are shown in central axial plane through the US array.

Based on the geometry and element layout, phase delays were computed for ExAblate 2100. With these phase values, the array elements were excited at uniform signal amplitude to obtain

- planar sonication (iso-phase or synchronous operation)
- diverging beam pattern (60^o angle)
- curvilinear or cylindrically focused beam pattern (40 mm focal depth along the array elevation)
- electronically scanned curvilinear beam patterns (three time multiplexed focal positions at 40 mm depth and 5 mm, 0, -5 mm azimuth)

ExAblate 2100 was operated in a low-intensity (0.86 W/cm2), CW (3 min) mode. Sonications in tissue-mimicking phantoms were monitored using multi-plane MR thermometry. 2 – 6 ^{o}C temperature rises were recorded during all sonications, with low measurement artifacts (examples shown in Figure 4b and Figure 4c). The azimuthal/angular expanse of temperature distribution was controlled through beamforming. Maximum width of 4 ^{o}C contour (corresponding to 41 ^{o}C in a clinical case) was 2.4 cm for planar, 3.6 cm for diverging, 0.5 cm for curvilinear and 3 cm for scanned sonication patterns.

4. SUMMARY

Simulations and preliminary experiments demonstrate the feasibility of delivering mild hyperthermia to the prostate with ExAblate 2100 ERUS prostate ablation system. Phased array beamforming techniques may be used to tailor acoustic energy deposition pattern in 3D, along array length and angular expanse. Hyperthermia-specific phasing was implemented on the ExAblate system and continuous wave sonications generated therapeutic temperature rises during phantom experiments. MRTI could be accurately performed with low artifacts during such prolonged sonications. Within

hardware and software constrains imposed by the ERUS array design, it may be possible to administer protracted hyperthermia to posterior quadrants or hemi-gland prostate.

Inverse planning algorithms developed for phased array hyperthermia can be applied to this scenario to optimize beamforming schemes.[19-21] Such planning was beyond the scope of this initial study, but will be implemented in future investigations. Clinical trials for prostate ablation using the ExAblate 2100 system are already underway. As shown in this study, it can be modified for mild hyperthermia delivery under MR-guidance. ERUS-based hyperthermia with precise tumor targeting can be combined with hypofractionated SBRT high dose rate radiation treatments.[22] It may be also be used in conjunction with temperature sensitive liposomes for targeted delivery of anti-cancer drugs to focal tumors.[6, 13] The treatment may be potentially extended to other tumor sites in the pelvic cavity, such as rectum and anal canal, and uterine cervix.

ACKNOWLEDGEMENTS

This study was supported by grants from Focused Ultrasound (FUS) foundation and National Institutes of Health (NIH) (R01CA122276, R01CA111981).

REFERENCES

[1] Wust P, Hildebrandt B, Sreenivasa G, Rau B, Gellermann J, Riess H, et al, "Hyperthermia in combined treatment of cancer," The lancet oncology 3(8), 487-497 (2002).

[2] Van der Zee J, "Heating the patient: a promising approach?," Annals of oncology, 13(8), 1173-1184 (2002).

[3] Leopold KA, Dewhirst MW, Samulski TV, Dodge RK, George SL, Blivin JL, et al, "Cumulative minutes with T_{90} greater than $temp_{index}$ is predictive of response of superficial malignancies to hyperthermia and radiation," International Journal of Radiation Oncology Biology Physics 25(5), 841-847 (1993).

[4] Franckena M, Fatehi D, Bruijne M, Canters RAM, Norden Y, Mens JW, et al, "Hyperthermia dose-effect relationship in 420 patients with cervical cancer treated with combined radiotherapy and hyperthermia," European Journal of Cancer 45(11), 1969-1978 (2009).

[5] Diederich CJ, Wootton J, Prakash P, Salgaonkar V, Juang T, Scott S, et al, "Catheter-based ultrasound hyperthermia with HDR brachytherapy for treatment of locally advanced cancer of the prostate and cervix," Proc: SPIE 79010, 79010O-79010O-8 (2011).

[6] Needham D, Dewhirst MW, "The development and testing of a new temperature-sensitive drug delivery system for the treatment of solid tumors," Advanced drug delivery reviews 53(3), 285-305 (2001) .

[7] Diederich CJ, Hynynen K, "Ultrasound technology for hyperthermia," Ultrasound in medicine & biology. 25(6), 871-887 (1999).

[8] Hutchinson E, Dahleh M, Hynynen K, "The feasibility of MRI feedback control for intracavitary phased array hyperthermia treatments," International journal of hyperthermia. 14(1), 39-56 (1998).

[9] Smith NB, Buchanan MT, Hynynen K, "Transrectal ultrasound applicator for prostate heating monitored using MRI thermometry," International Journal of Radiation Oncology Biology Physics 43(1), 217-225 (1999).

[10] Hurwitz M, Kaplan I, Svensson G, Hansen M, Hynynen K, "Feasibility and patient tolerance of a novel transrectal ultrasound hyperthermia system for treatment of prostate cancer," International journal of hyperthermia 17(1), 31-37 (2001).

[11] Jolesz FA, Hynynen K, McDannold N, Tempany C, "MR imaging-controlled focused ultrasound ablation: a noninvasive image-guided surgery," Magnetic resonance imaging clinics of North America 13(3), 545 (2005).

[12] Mu Z, Ma C, Chen X, Cvetkovic D, Pollack A, Chen L, "MR-guided pulsed high intensity focused ultrasound enhancement of docetaxel combined with radiotherapy for prostate cancer treatment," Physics in medicine and biology 57(2), 535 (2012).

[13] Partanen A, Yarmolenko PS, Viitala A, Appanaboyina S, Haemmerich D, Ranjan A, et al, "Mild hyperthermia with magnetic resonance-guided high-intensity focused ultrasound for applications in drug delivery," International Journal of Hyperthermia 28(4), 320-336 (2012).

[14] Ocheltree KB, Frizzel L, "Sound field calculation for rectangular sources," IEEE Transactions on Ultrasonics Ferroelectrics and Frequency Control 36(2), 242-248 (1989).

[15] Lagendijk J, "Hyperthermia treatment planning," Physics in medicine and biology 45(5), R61 (2000).
[16] Wootton JH, Ross AB, Diederich CJ, "Prostate thermal therapy with high intensity transurethral ultrasound: The impact of pelvic bone heating on treatment delivery," International Journal of Hyperthermia 23(8), 609-622 (2007).
[17] Goss S, Johnston R, Dunn F, "Comprehensive compilation of empirical ultrasonic properties of mammalian tissues," The Journal of the Acoustical Society of America 64(2), 423 (1978).
[18] Hynynen K, DeYoung D, "Temperature elevation at muscle-bone interface during scanned, focused ultrasound hyperthermia," International journal of hyperthermia 4(32), 267-279 (1988).
[19] Ebbini ES, Cain CA, "Multiple-focus ultrasound phased-array pattern synthesis: optimal driving-signal distributions for hyperthermia," IEEE Transactions on Ultrasonics Ferroelectrics and Frequency Control 36(5), 540-548 (1989).
[20] McGough RJ, Ebbini ES, Cain CA, "Direct computation of ultrasound phased-array driving signals from a specified temperature distribution for hyperthermia," IEEE Transactions on Biomedical Engineering 39(8), 825-835 (1992).
[21] Daum D, Hynynen K, "Theoretical design of a spherically sectioned phased array for ultrasound surgery of the liver," European journal of ultrasound 9(1), 61-69 (1999).
[22] Hurwitz MD, "Today's thermal therapy: not your father's hyperthermia: challenges and opportunities in application of hyperthermia for the 21st century cancer patient," American journal of clinical oncology 33(1),96 (2010).

Model-based feasibility assessment and evaluation of prostate hyperthermia with a commercial MR-guided endorectal HIFU ablation array

Vasant A. Salgaonkar[1*], Punit Prakash[2], Viola Rieke[3], Eugene Ozhinsky[3], Juan Plata[4], John Kurhanewicz[3], I-C (Joe) Hsu[1], Chris J. Diederich[1]

[1]Thermal Therapy Research Group, Radiation Oncology, University of California San Francisco
1600 Divisadero St., Suite H-1031, San Francisco, CA USA 94143
Tel: +1 – 415 – 353 – 9852
*Email: salgaonkarv@radonc.ucsf.edu

[2]Electrical and Computer Engineering, Kansas State University
2077 Rathbone Hall, Manhattan, KS 66506, USA

[3]Radiology and Biomedical Imaging, University of California San Francisco
505 Parnassus Ave., San Francisco CA USA 94143

[4]Radiology, Stanford University
1201 Welch Rd. Stanford CA USA 94305

Running title: Prostate hyperthermia with a commercial MR-guided HIFU ablation array

Keywords: hyperthermia, MR-guided HIFU, endorectal ultrasound, phased array, beamforming, modeling, simulation.

Abstract

Purpose: Feasibility of targeted and volumetric hyperthermia (40 - 45 ^{o}C) delivery to the prostate with a commercial MR-guided endorectal ultrasound (MRgERUS) phased array system, designed specifically for thermal ablation and approved for ablation trials (ExAblate 2100, Insightec Ltd.), was assessed through computer simulations and tissue-equivalent phantom experiments with intention of fast clinical translation for targeted hyperthermia in conjunction with radiotherapy and chemotherapy.

Methods: The simulations included a 3D finite element method (FEM) based biothermal model, and acoustic field calculations for the ExAblate ERUS phased array (2.3 MHz, 2.3×4.0 cm^2, >1000 elements) using the rectangular radiator method. Array beamforming strategies were investigated to deliver protracted, continuous-wave hyperthermia to focal prostate cancer targets identified from representative patient cases. Constraints on power densities, sonication durations and switching speeds imposed by ExAblate hardware and software were incorporated in the models. Preliminary experiments included beamformed sonications in tissue mimicking phantoms under MR temperature monitoring at 3 T (GE Discovery MR750W).

Results: With T_{max}<45 ^{o}C, T>41 ^{o}C was calculated in 13–23 cm^3 volumes for sonications with planar or diverging beam patterns at 0.9–1.2 W/cm^2, in 1.5-4 cm^3 volumes for simultaneous multi-point focus beam patterns at 2 – 3.4 W/cm^2, and in ~6.0 cm^3 for curvilinear (cylindrical) beam patterns at 0.75 W/cm^2. Focused heating patterns may be practical for treating focal disease in a single posterior quadrant of the prostate and diffused heating patterns may be useful for heating quadrants, hemi-gland volumes or even bilateral targets. Treatable volumes may be limited by pubic bone heating. Therapeutic temperatures were achieved for a range of physiological parameters, sonication duty cycles and rectal cooling. Phasing patterns implemented on the ExAblate prostate array produced 4-12 ^{o}C temperature rises during phantom experiments (~0.86 W/cm^2, 15 min).

Conclusions: The ExAblate 2100, designed specifically for thermal ablation, can be controlled for delivering continuous hyperthermia in prostate to augment radiotherapy and drug delivery, while working within operational constraints.

55

INTRODUCTION

Hyperthermia has been combined successfully with several cancer treatment modalities, such as radiation therapy, chemotherapy and hormonal therapy, and is known to improve treatment outcomes (1-6). Mild hyperthermia (40 – 45 ^{o}C) can induce direct cytotoxicity in tumors, radiosensitize cancer cells by impairing DNA repair mechanisms, and enhance blood flow in tumor microenvironments to increase tumor oxygenation and facilitate drug delivery (7). It may also be used to enhance localized drug delivery (8) and gene therapy (9) as reported in some recent investigations. Hyperthermia treatment can be administered by applicators that deliver radiofrequency energy, microwaves, or ultrasound energy (10-12). These devices may be designed for extracorporeal placement, intracavitary or endoluminal deployment, or interstitial or percutaneous insertion (13-15). Typically, these treatments involve heating tumor targets for 30 – 60 min duration. For maximum clinical benefit, uniform temperature profiles are desired within target volumes, with minimum temperature greater than 40 ^{o}C and 6 – 10 min cumulative thermal dose at 43 ^{o}C (16-18). Administering hyperthermia to tumors situated deep inside the body presents significant clinical challenges such as, selective energy deposition within the tumor while thermally sparing surrounding structures, and sufficient thermometry for reliable treatment monitoring (19, 20). Such difficulties may be encountered during hyperthermia delivery to focal cancer targets in prostate and other organs inside the pelvic cavity.

Endorectal ultrasound (ERUS) transducer arrays have been investigated for hyperthermia delivery to the prostate and studies devoted to design and pre-clinical evaluation of such devices have been reported (21-26). Clinical studies have demonstrated feasibility of safe, reliable and effective application of prostate hyperthermia with ERUS applicators (27-30). Currently, MR guided high intensity focused ultrasound (MRgHIFU) systems are being increasingly utilized for noninvasive or minimally-invasive thermal ablation of soft tissue tumors in multiple organ sites (31, 32). Typically, these are multi-element phased array applicators capable of delivering ultrasound energy with precise spatial control. Integration with MRI and MR thermometry has enabled real-time guidance and monitoring of HIFU ablation procedures (33). Endorectal

ultrasound applicators, consisting of phased arrays or multi-sectored devices, have been investigated for delivering hyperthermia under MR guidance and control (25, 26, 34).

Recent studies have utilized MR-guided HIFU systems for enhancement of drug delivery in cancer treatment. This has been achieved through pulsed mode operation of the HIFU system (35-37), rapid mechanical (38) or electronic translation (39) of the HIFU focus, or simultaneous multi-point focusing of HIFU phased array (34) to heat small volumes. Enhancement in uptake of free-flowing (35-37) and liposome-encapsulated drug has been achieved (38, 39).

ExAblate 2100 (InSigtec Ltd.) is a commercially available MR-guided thermal ablation system. It consists of an ERUS phased array designed for prostate ablation (Figure 1a). Treatments are planned using detailed anatomical MR images that facilitate identification of target zones, and help in ERUS array placement and orientation. Based on real time MR temperature imaging (MRTI), the ERUS array can be utilized to translate a small HIFU focal pattern in 3D and perform repetitive ablations to coagulate overlapping lesions that will cumulatively cover the entire target volume (40, 41). In contrast to HIFU, hyperthermia requires more diffused energy deposition sustained over longer durations to establish uniform temperature distribution and sufficient thermal dose within the entire targeted volume. Array beamforming and phasing requirements of these sonications are very different from conventional HIFU exposures (Figure 1b, Figure 2a). Hence, in this study, the feasibility of protracted hyperthermia to prostate targets (focal targets, posterior quadrants, hemi-gland) with the ExAblate 2100 array was assessed through simulations, modeling and preliminary experiments. Operational modifications required for continuous wave (CW) sonications, unlike previous studies where pulsed-HIFU was utilized to maintain hyperthermic temperatures (35-37), and continuous volumetric multi-plane MRTI were identified within system hardware and software constraints.

The ExAblate 2100 system is already in clinical trials for prostate ablation (40-42). If it can be successfully adapted for protracted hyperthermia, it can be potentially fast-tracked for clinical application. With this motivation, this initial study employed theoretical and

experimental techniques to identify operational modifications, and assess the feasibility and capability of safe and reliable MR-guided prostate hyperthermia with the ExAblate 2100 prostate applicator.

METHODS

In this study we utilized computer simulations and thermal dosimetry experiments to assess the feasibility of prostate hyperthermia with the ExAblate 2100 MRgERUS phased array. The simulation studies consisted of acoustic pressure calculations, and array beamforming for generating hyperthermia-specific US energy deposition patterns. Biothermal models were employed to ascertain US-induced heating for the various sonication strategies considered. Clinical images were used to generate anatomical geometries and FEM meshes for representative patient datasets. The initial experiments were employed to demonstrate implementation of hyperthermia-specific sonication strategies on the ExAblate phased array ablation system.

Acoustic power deposition calculations

Acoustic calculations were performed for the ExAblate 2100 prostate phased array. To ensure realistic modeling, all array design specifications and details provided by Insightec Ltd. were incorporated. This included operating frequency (2.3 MHz), array dimensions (23×40 mm^2) independent power channels (~1000), individual rectangular element size, proprietary element layout and electrical connection scheme which includes clustering of distributed elements to have same phasing, phase encoding and round-offs, sonication intensities and sonication duration limitations, duty cycles, and software constraints.

The acoustic pressure field from an individual array element was computed using the rectangular radiator method developed by Ochletree and Frizzel (43). Considering each element as a simple rectangle-shaped baffled piston source, the cumulative acoustic pressure (p_0) generated in a lossless aqueous medium because of continuous wave excitation of N elements can be calculated using the following equation.

$$p_o(x,y,z) = \frac{j\rho c\Delta A}{\lambda}\sum_1^N \frac{u_n}{R} e^{-jkR} sinc\left[\frac{k(x-x_n)\Delta w}{2R}\right] sinc\left[\frac{k(y-y_n)\Delta h}{2R}\right] \quad (1)$$

In Eq. 1, the phased array transducer is assumed to be in plane $z = 0$, ρ is the density, c is the speed of sound, λ is the wavelength, k is the wave-number, $u_n = |u_n| \times \exp(-j\varphi_n)$ is the complex particle velocity at the surface of the n^{th} element and φ_n is the phase, Δw, Δh, ΔA are the width, height and surface area of an element respectively , x_n and y_n are the centers of the n^{th} element, and $R = [(x-x_n)^2 + (y-y_n)^2 + z^2]^{0.5}$. The accuracy of the sinc function approximation in Eq. 1 is dictated by the expression $\Delta w \leq (4\lambda z/F)^{0.5}$, where a larger value of F implies greater accuracy in pressure estimation at a given distance of z. For the simulation space in this study, dimensions of the square array elements and the operating frequency, F always exceeded 150.

The acoustic energy (Q_{ac}) deposited at a point in the simulation space is given in Eq. 2.

$$Q_{ac}(x,y,z) = 2 \propto (x,y,z) \frac{|p_0(x,y,z)|^2}{2\rho c} exp\left[-2z \int_0^z \mu(z) \cdot dz\right] \quad (2)$$

In Eq. 2, p_0 is peak pressure, α is acoustic absorption, μ is acoustic attenuation, ρ is density, and c is sound speed. An averaged acoustic attenuation was applied along the ultrasonic beam path. All scattered energy was assumed to be absorbed locally. 60% transmission of longitudinal acoustic waves was assumed at the bone-tissue interface (more details in patient specific modeling that follows) with reflection, refraction and shear wave conversion being neglected (44). Modeling constants related to acoustic properties of tissues have been compiled in Table 1.

Array Beamforming

To modify/tailor energy deposition patterns, ERUS elements were excited with specific phase delay values. These values were computed based on element position and focusing characteristics required to generate the requisite beam patterns. Phasing schemes investigated in this study are described next. In this description, azimuth refers to dimension along array length (40 mm), elevation refers to the dimension along array width (23 mm), and range or depth refers to orthogonal distance from the array surface.

Multi-point focusing: To selectively heat small targets, such as localized focal cancer targets located in the posterior peripheral zone of the prostate (10 – 15 mm wide, 1 – 2 cm^3 volume),

beamforming techniques which simultaneously focus the ERUS array at multiple (4 - 8) points were explored (Figure 3a). In clinical scenarios considered here, cancer targets were located at a distance of 10 – 20 mm from the rectal wall and 25 – 35 mm from the ERUS array (accounting for ~15 mm radius of the cooling balloon). Hence, the array focus points were placed between 25 – 35 mm depth and 5 – 10 mm transverse distance from the array axis. For such focusing, phase delays were first computed for all channels in order to focus the array at each individual focusing point. An averaged set of phase values was then computed and applied to the array elements.

Cylindrical or curvilinear focusing: To simulate focusing behavior of a curvilinear or cylindrically focused transducer, the ERUS array was focused along the array elevation direction (Figure 4a). Phase delays were computed based only on the distance between ERUS elements and a cylindrical focus axis (based only on the focusing depth and element elevation). Here the focusing depth was set between 25 – 35 mm for delivering zonal hyperthermia (10 – 15 mm wide targets) along the prostate length.

Diverging sonications: This approach was explored to heat wide focal targets near the posterior periphery of the prostate or posterior quadrant of the gland. To heat such target, the synthetic focusing point of the array was placed 10 – 60 mm behind the array along the entire array elevation. Phase delays were again computed using only the focusing depth and elevation position of the array elements. This scheme was employed to generate defocused or cylindrically diverging wavefronts (Figure 5a) that may heat targets close to the array but wider than its elevation dimension (23 mm).

Planar sonications: Planar beam patterns were simulated by setting uniform phase values for all power channels (Figure 6a). This achieved the effect of synchronous operation of all ERUS array elements to mimic the functionality of a planar rectangular transducer with a large aperture. These sonications were explored for hyperthermia to hemigland prostate or posterior quadrants of the gland.

Biothermal Models

Heat transfer was modeled using the Pennes bioheat equation as shown below (45).

$$\rho c_{pt} \frac{\partial T'}{\partial t} = \nabla \cdot [k_t \nabla T'] - \omega_b c_{pb} T' + Q_{ac} \quad (3)$$

In eq. 3, ρ is the density, c_{pt} and c_{pb} are specific heat capacity values for tissue and blood respectively, k_t is thermal conductivity, T' is the temperature rise over basal/blood temperature, ω_b is the blood perfusion and Q_{ac} is the heat generated due to acoustic energy deposition. Modeling constants related to thermal properties of tissues have been compiled in Table 1.

Model geometry

The biothermal models were employed to calculate temperature profiles on generalized and patient-specific geometries. Acoustic intensity was varied to achieve a maximum temperature close to 45 ^{o}C, and dimensions of resulting simulated 40 ^{o}C and 41 ^{o}C temperature clouds were computed.

Generalized model geometry consisted of the ERUS phased array situated inside a 15-mm radius cylindrical balloon filled with degassed water sonicating homogenous soft tissue. For these models physiological parameters, such as blood perfusion, acoustic parameters and thermal properties of soft tissue were assumed to be homogeneous.

Patient specific model geometry was created from two representative patient data sets (example shown in Figure 1(b) and Figure 2(a)). Critical organ structures such as the prostate and cancer target volume, bladder, rectum, urethra and pubic bones were manually segmented from serial MR or CT axial images by using contouring tools available in a radiation therapy treatment planning program (Oncentra, Netherlands) and a 3D modeling software (Mimics and 3-Matic, Materialise, Belgium). Both patients had focal prostatic tumor nodes in the posterior peripheral zone near the gland apex. The first patient had a unilateral target confined to the right side (prostate volume = 22 cm^3, tumor volume = 1.2 cm^3). The second patient had a bilateral

target, but predominantly on the left (prostate volume = 19 cm^3, target volume = 1 cm^3). Due to the high acoustic absorption of bone and acoustic penetration depth at 2.3 MHz, acoustic energy may cause some heating in the pubic symphysis located anterior to the gland. To study the impact of bone heating on treatment quality, patient cases were selected with pubic bone located far (25 – 30 mm, case 1) or near the gland (8 – 10 mm, case 2). The ERUS phased array was assumed perfectly coupled to the rectal wall by a distensible cooling balloon that contained temperature-regulated circulating water for cooling of rectal tissue, and protection of the phased array. Position and orientation of the ERUS phased array was set to direct acoustic energy at the target volume. In a treatment scenario with the ExAblate ERUS array, such positioning would be achieved using translation and rotation module of the ExAblate system. Bladder was assumed to contain water and urethral cooling was applied as required.

Boundary conditions

For both generalized and patient-specific geometries, the outer simulation boundaries were assumed to have constant temperature, which was set to the same value as blood/basal temperature (37 ^oC). The ERUS cooling balloon and urethral cooling balloon were modeled to have constant temperature dictated by cooling water flow (T_{cool} = 22 – 41 ^oC).

Numerical evaluation

The biothermal and acoustic models were evaluated using COMSOL Multiphysics 3.5a and 4.3 (Comsol Inc., Burlington, MA), a finite-element method (FEM) software program, and Matlab 7.5 (MathWorks Inc., Natick, MA). Patient specific geometry was created by converting the segmented organ contours to 3D volumes using Mimics (Materialise, Belgium) and then to FEM mesh using 3-Matic (Materialise, Belgium) software packages. The FEM mesh parameters, in terms of mesh element dimensions, were selected through an iterative process to ensure a stable thermal solution. Implicit FEM solvers (PARDISO for steady state solutions and geometric multigrid for transient solutions), available within COMSOL Multiphysics, were utilized. In the generalized models, mesh element sizes <1.5 mm were employed close to the applicator cooling balloon and mesh element sizes <1.2 mm were employed between 5 – 25 mm axial distance from

the ERUS array. The latter corresponds to the region where maximum heating occurs. In the patient specific models, mesh element sizes were <1.8 mm near the applicator and rectum, <1 mm within cancer target, and <1.5 mm near the proximal bone surface.

Steady state implementation of Eq. 3 was utilized during all patient-specific models. The generalized models employed steady state or transient version (**Figure 7**) of Eq. 3. The generalized models were also used for a parametric study that investigated the impact of blood perfusion, applicator cooling and sonication duty cycle on heating performance of the array.

Evaluation in Tissue Phantom under MRTI

To demonstrate beamforming strategies developed in the simulation studies, some hyperthermia-specific sonications were implemented on ExAblate 2100 ERUS phased array ablation system. Phasing patterns, specific to the proprietary layout of the ERUS array, were applied to the phased array using research GUI and tools provided in the InSightec ablation system. This research version consists of utility interfaces (CPC 5.3.2) which allow the ablation system to be programmed with greater flexibility. Through these GUI packages, it is possible to set sonication parameters such as input power and exposure time, and also implement customized beamforming patterns on the system.

In the preliminary tests presented here, the ExAblate prostate array was employed to heat tissue-mimicking phantoms provided for quality assurance and calibration by InSightec (Model TXS-100, ATS Laboratories, Inc, Bridgeport, CT). The phantom was shaped like a lightly tapered cylinder ~10.2 cm in diameter and ~12.7 cm in height with acoustic attenuation = 0.503 dB/cm/MHz and sound speed = 1538 m/s (46). Experiments were conducted in a 3 T MRI scanner (GE Healthcare Discovery MR750W) where imaging and temperature data was obtained by a birdcage head coil (GE). Complex MR images were acquired in multiple imaging planes for MRTI, with all slices in the same orientation. For the data presented here, image slices were either in axial or coronal orientation. Five axial planes were recorded with slice thickness of 5 mm, inter-slice spacing of 1.0 mm and the center slice was positioned at the array center. Five coronal planes were recorded with slice thickness of 5 mm, inter-slice spacing of 0.5 mm and the

center slice was positioned at the 35 mm distance from array surface. MRTI was performed using a spoiled gradient echo sequence with the following imaging parameters: TE = 16 ms, BW = +/- 31.2 kHz. The FOV was 14 cm, slice thickness = 5 mm, flip angle = 30, and matrix size = 256×256 pixels. The complex images were transferred to a workstation in real-time and temperature images were reconstructed with the proton resonance frequency (PRF) method (47).

For these initial experiments, conservative exposure parameters were employed. Electrical power was set at 10 W (surface acoustic intensity ~ 0.86 W/cm^2). For this power level, operational constraints of the ExAblate 2100 system only allowed sonication durations of 5 min. Three sets of such 5-min sonications were conducted to obtain a total heating time of 15 minutes. Time duration between consecutive sonications was 5 – 10 s. After a single sonication, the system required re-initialization and it resulted in this short time delay between consecutive sonications. To ensure safe operation and protection of the prostate array, cooling water (22 ^{o}C) flow was maintained throughout the exposures (Figure 8).

RESULTS

Acoustic Calculations

Acoustic fields for various focusing patterns were calculated to investigate simultaneous multi-point focusing and shaped energy deposition patterns for generating hyperthermia. Calculated acoustic fields indicated that the ExAblate ERUS array was capable of creating tight focal spots along its axis. The 3-dB beam-width for focusing depths of 20 – 40 mm was 0.6 – 1.15 mm in the elevation dimension and 0.4 – 0.65 mm in the azimuth dimension. Off-axis focusing resulted in some energy deposition in the side lobes. The ratio of maximum acoustic intensity values in the side lobe and the main lobe was computed in the focusing plane and was used to quantify capability for off-axis focusing and beam steering. At a focusing depth of 20 mm and off-axis focusing position of 5 – 10 mm, maximum energy in the side lobe was 5 – 20.0% of maximum energy in the main lobe. At a 30 mm depth, this proportion was 2.5% – 15.5% and at 40 mm depth it was 1.4% - 6.0%. Similar trends were observed when curvilinear focusing was employed. When focused in the elevation dimension, focusing depths below 25 mm resulted in peak side-lobe intensity values in excess of 10% of peak intensity in the main lobe.

Generalized Models

Therapeutic volumes V_{40} and V_{41} (volumes of iso-thermal clouds of 40 ^{o}C and 41 ^{o}C respectively) were determined for different sonication/beamforming strategies and the results are presented in Table 2 - Table 5 from. For these models, the input power was empirically adjusted to obtain a maximum temperature in the range of 44.5 – 45 °C, within operational limits of the ERUS array (surface acoustic intensity < 3.4 W/cm^2). A constant blood perfusion rate of 2 kg/m^3/s was assumed for these models. With simultaneous multi-point focusing V_{40} and V_{41} were small. For 4 – 8 focusing points, V_{40} was between 3.8 – 7.2 cm^3 and V_{41} was between 1.5 – 3.9 cm^3. For 8-point sonications, using the maximum allowed acoustic intensity resulted in T_{max} < 43 ^{o}C. With curvilinear focusing in elevation direction at depth of 25 and 35 mm along the propagation axis, V_{40} = 12 cm^3 and V_{41} = 6 cm^3, respectively, were calculated. Larger treatable volumes were

calculated for diffused sonications. With diverging and planar patterns, V_{40} = 24 - 35 cm^3 and V_{41} = 12 - 22 cm^3 were computed.

Parametric Analysis

Results from a parametric study utilizing planar sonications are presented in Table 6 - Table 8. Impact of blood perfusion variation on heating performance was studied by changing perfusion between 0.5 - 8.0 $kg/m^3/s$. The input acoustic intensity was varied with perfusion between 0.61 - 2.15 W/cm^2 to maintain maximum temperature close to 45 °C. Dimensions of the 40 and 41 °C iso-temperature contours were computed. In the azimuthal direction (along applicator width), dimensions of these contours varied from 33 - 26 mm and 27 - 22 mm, respectively, with increasing perfusion. In the elevation direction (along applicator length), variations in contour dimensions were lower, spanning 40 - 37 mm and 35 - 33 mm. Depth of tissue heating for both contours were 71.5 - 69 mm and 67 - 59 mm. For these models, applicator cooling was held constant at 30 ^oC.

The impact of applicator cooling for long duration sonication with the ExAblate 2100 array was studied by varying T_{cool} between 22 - 35 °C for planar sonication configuration discussed above (Table 7). Perfusion was held constant at 2.0 $kg/m^3/s$. Across the range of T_{cool} values considered, slight changes in applied power ranging from 1.05 - 0.92 W/cm^2 were needed to maintain T_{max} ~ 45 °C. With changes in T_{cool}, dimensions of the 40 °C and 41 °C contours showed minimal changes (< 2 mm) in azimuth or elevation dimensions. In the range dimension, reduced cooling caused some reduction in heating depth.

Hardware constraints imposed on the ExAblate 2100 system for applicator protection during long duration sonications, may require shorter duty cycles instead of continuous sonication. Hence, transient models employing planar sonications were implemented to study the impact of duty cycle variation on heating performance. Duty cycle was varied between 80%, 88% and 100% with pulse repetition frequencies of 0.0104 Hz, 0.011 Hz and CW. The blood perfusion rate was set to 2.0 $kg/m^3/s$ and T_{cool} was held constant at 30 °C. Peak acoustic intensity was varied such that the total energy delivered in a single pulse cycle was constant and the

maximum temperature was close to 45 °C. After 12 minutes into the treatment, steady temperature levels were achieved with 100% duty cycles. After this time instance, the observed temperature ripple in T_{max} was below 0.1 °C and 0.3 °C for the 88% and 80% duty cycle cases, respectively. Similar small ripples were also seen in iso-temperature volumes (Figure 7). For this comparison, dimensions of volume contours for thermal doses of 6 and 10 CEM43 were also calculated. For 100%, 88% and 80% duty cycles, the iso-dose cloud dimensions were within a millimeter agreement (Table 8).

Patient-specific Models

Multi-point focusing: An example of such multi-point focusing is shown in Figure 3, where conformal hyperthermia to a small focal target in right posterior quadrant of the prostate was simulated (patient case 1). For this preliminary effort, focal point placement was ascertained through a manual iterative process to maximize target coverage. The ERUS array was simultaneously focused on 6 points at an axial depth of 35 mm (Figure 3a). Foci were placed in the transverse plane such that the resultant heating best conformed to the target region shape. In the example shown here, acoustic intensity was 3.4 W/cm^2 (electrical power ~ 40 W) and maximum temperature was 44.5 °C.

Cylindrical or curvilinear focusing: The example shown in Figure 4 shows curvilinear focusing employed to target the cancer site from patient case 1. In this case, the focusing axis was placed along the array azimuth and the focal depth was 35 mm from the array surface. This sonication pattern allowed heating in wedge-shaped patterns. The input was set to 0.7 W/cm^2 acoustic intensity (electrical power ~ 8 W), which yielded a maximum temperature of 45 °C.

Planar sonications: Planar beam patterns were simulated by setting uniform phase values for all power channels. This achieved the effect of synchronous operation of all ERUS array elements to mimic the functionality of a planar rectangular transducer with a large aperture (Acoustic: 1.2 W/cm^2 or Electrical ~ 14 W). As shown in Figure 5, diffused energy deposition spread out over a larger volume was possible with this configuration. For this representative case, therapeutic

hyperthermia could be delivered to targets in the posterior quadrant of the prostate could be treated, extending to the prostate boundary.

Diverging sonications: Diverging acoustic beam patterns were simulated to heat wide targets in posterior prostate (Figure 6). Patient specific models were used to explore the possibility of heating bilateral targets with this configuration. The representative case shown in **Figure 6** contains a target primarily in the left posterior quadrant with a section extending past the urethra into the right quadrant. To heat this target, the synthetic focus was placed 10 mm behind the array along the entire array elevation. This resulted in wave fronts similar to tubular transducer elements (cylindrically diverging or defocused). As compared to the planar sonication strategy, angular expanse of energy deposition across the array azimuth was increased. However, higher input power (Acoustic: 1.35 W/cm^2, Electrical ~ 16 W) was required to achieve therapeutic temperatures. Also, energy deposition in the side lobes was more difficult to control.

Evaluation in Tissue Phantom under MRTI

Based on the proprietary irregular transducer element layout and wiring scheme of the ExAblate 2100 array, phasing patterns were calculated to generate the following sonication patterns and applied within phantom to evaluate generated temperature distributions (Figure 8).

- Planar sonication was performed using iso-phase/synchronous excitation of the transducer array elements. This was similar to placing a single focal point at a very large distance from the array and resulted in heating volumes close to the array determined by the width of the array.
- Diverging pattern was created by placing the synthetic focus 20 mm behind the array, on its axis and along array elevation dimension. This caused heating in a cylindrically defused volume with its extent greater than the array width.
- Curvilinear pattern with synthetic focus at 35 mm distance on the array axis, and along array elevation dimension. This resulted in wedge shaped heating volumes caused by cylindrical focusing.

- Simultaneous multipoint focusing was demonstrated using 6-point focusing pattern applied in the simulation example shown earlier (Figure 3). The six foci were placed at 35 mm distance from the array. The heating pattern was created to treat gibbous target shapes. This is evident from the irregular shaped temperature distribution seen in the coronal plane.

Phase delays associated with these beamformed sonications were programmed into the ExAblate system using the CPC software interface. Figure 8 depicts temperature profiles in tissue mimicking phantoms showing up to 12 °C temperature rises after 15 min heating with a relatively low power setting of 0.86 W/cm^2 (acoustic). MRTI was performed with minimum measurement artifact. These preliminary experiments illustrate the ability to successfully employ beamforming to control the shape of energy deposition and resulting heat generation, and to deliver long duration power output with the ExAblate 2100 MRgERUS system.

DISCUSSION

Feasibility of adapting the ExAblate 2100 ERUS ablation array within its hardware, software and operational constraints for delivering protracted mild hyperthermia to contiguous volumes in the prostate has been examined through simulations and preliminary experiments. Array beamforming can be utilized effectively to tailor energy deposition based upon the size and location of target volumes. Appropriate phasing patterns can enable targeting specific volumes in the posterior region of the gland, posterior quadrant hyperthermia and hemi-gland hyperthermia. Simultaneous multipoint focusing and curvilinear focusing can be employed to heat small targets (1.5 – 6.6 cm^3). With these sonications, energy can be delivered selectively with tailoring along the array length and in axial distance. Wide targets in the posterior prostate can be effectively heated using divergent/diffuse sonications. These along with planar sonications may be effective in delivering quadrant or hemi-gland hyperthermia to large contiguous volumes (13.3 – 22.8 cm^3). Initial experiments in tissue mimicking phantoms demonstrated the feasibility of implementing hyperthermia-specific array beamforming on the ExAblate array and delivery of protracted continuous wave sonications to generate hyperthermia in contiguous volumes under MRTI.

ExAblate 2100 has approval for clinical trials pertaining to prostate ablation (40-42). Potentially, it can be fast tracked into the clinic for hyperthermia applications as well. Feasibility of safe hyperthermia delivery to the prostate using transrectal ultrasound arrays (~1.5 MHz, 4 – 16 elements) has been reported in the past (28 - 30). Diverging sonications with ExAblate array can be used to deliver diffuse hyperthermia similar to cylindrical-element applicators described in the aforementioned studies. Greater control of heating may be possible due to greater array beamforming possibilities arising from larger number of elements, mechanical rotation and translation capabilities, and volumetric thermal dosimetry through MR temperature monitoring. This may enable precise energy delivery to the prostate while limiting thermal dose to critical structures such as urethra, neurovascular bundles and pubic bones.

Some recent studies have reported hyperthermia delivery to small tissue volumes using commercial MR-guided extracorporeal HIFU ablation applicators. These studies consisted of animal experiments designed to study enhanced delivery and uptake of drugs using sub-lethal thermal doses. In refs. (35-37), extracorporeal phased array included in ExAblate 2000 by InSightec was employed for pulsed-HIFU sonications in small (~45 mm^3) implanted murine tumors under MR-guidance with the goal to cause mild temperature increases. These sonications were only limited to sequential focusing at multiple points, available as part of ablation tools within the ExAblate system. Short duty cycles were employed to limit temperature rises. CW sonications which employ electronic and mechanical scanning of a single HIFU focus under MR-guidance have also been explored to deliver hyperthermia with another commercial ablation system (Sonalleve, Philips Medical Systems, Vantaa, Finland). The animal study in ref. (39) demonstrates treatment of small volumes (treatment cell diameter of 4 – 16 mm) with fast translation of the HIFU focus. In another study by the same group, multi-point focusing was implemented on the same HIFU system to treat target volumes with ~15 mm diameter (34).

The prostate array from ExAblate 2100 system is designed for endocavity placement as opposed to the external arrays employed in the aforementioned studies, and hence has stringent size and design constraints. Hyperthermia delivery to large treatment volumes with this small array requires more meticulous planning, but it can also offer therapeutic advantages. Targeted CW sonications to treat large and deep cancer targets are more feasible with an endocavity array because it is less susceptible to organ motion and intervening tissue structures as compared to an external applicator. Effective heating of larger volumes opens the possibility of heating hemi-gland prostate or bilateral targets. Simultaneous multi-focus beamforming can also be

implemented on InSightec prostate array to conformably heat smaller targets, and it can potentially produce more steady temperature profiles than electronic scanning of HIFU focus.

Array design constraints on the ExAblate 2100 prostate array such as element layout and element connections place limits on electronic scanning, focal gains and side-lobe generation when compared to ERUS arrays considered for hyperthermia during earlier studies (21 - 30). Whole gland hyperthermia may not be possible simply through beamforming alone. However, the ExAblate 2100 has a rotational and translational positioning module that affords accurate positioning and orientation of the applicator within the patient. Hence, lateral regions of the gland can be treated sequentially to effectively produce whole gland heating. Further, it may be possible to apply frequent and rapid mechanical translation/rotation of the applicator to combine electronic and mechanical scanning. However motion-associated artifacts in MR thermometry could be problematic and may require MR-thermometry techniques which employ multiple baseline images for reliable temperature measurements in such scenarios (48, 49).

The relatively small size and low operating frequency of the array also limits targeting capability. The array can be used more effectively to target cancer in the posterior periphery of the gland, however, focal gain is reduced when targeting volumes placed toward the anterior border (for depths of greater than 45 mm). The low frequency can also result in energy deposition anterior to the prostate gland, especially during hemi-gland heating. This may result in heat generation in the pubic bone, especially in cases where it is close (within 5 - 10 mm) to the prostate. As seen in the representative patient case 2 (Figure 6), where the pubic bone is less than 1 cm from the gland, undesired heating can occur in the bone. Urethral cooling may also be necessary when heating hemi-gland or quadrant volumes. The patient cases shown here have cancer targets at the posterior periphery of the prostate close to the rectal wall. Cooling flow

which protects the device and the rectum has to be carefully applied as excessive cooling can negatively impact hyperthermia delivery. Clinical hyperthermia treatments with this approach should be carefully planned taking these factors into consideration.

The ExAblate prostate array following operational modifications can be potentially used to exploit new treatment paradigms where hyperthermia may be combined with hypofractionated SBRT high dose rate radiation treatments (30, 50). It may be also be used in conjunction with temperature sensitive liposomes for targeted delivery of anti-cancer drugs to focal tumors (19, 39). Such transrectal hyperthermia delivery may be effective as part of multimodality regimens which incorporate chemotherapy and immunotherapy (51, 52) to treat advanced or salvage cases of prostate cancer. Transurethral (53) or transrectal (54) hyperthermia has also been employed for treating chronic prostatitis, and similar treatments may be possible with the InSightec prostate array. The ExAblate prostate array may be potentially extended to hyperthermia treatments of other tumor sites in the pelvic cavity, such as rectum and anal canal. Future investigations that would be useful for implementing hyperthermia with this system could include the development of inverse planning algorithms to optimize beamforming schemes (such as multi-focal patterns) specific for phased array prostate hyperthermia (55-57). Temperature-based feedback control methods could possibly be implemented to improve target heating and avail the full power of MRTI for full 3D volumetric temperature feedback.

CONCLUSIONS

Simulations and preliminary experiments demonstrate the feasibility of delivering protracted mild hyperthermia 40-45 ^{o}C for >15-30 min to the prostate with ExAblate 2100 ERUS prostate ablation system. Phased array beamforming techniques may be used to tailor acoustic energy deposition pattern in 3D, along array length and angular expanse. Hyperthermia-specific beamforming strategies were implemented on the ExAblate system and continuous wave sonications generated therapeutic temperature rises during phantom experiments. Within hardware and software constraints imposed by the ERUS array design, it may be possible to administer protracted hyperthermia to posterior quadrants or hemi-gland prostate.

ACKNOWLEDGEMENTS

This study was supported by grants from Focused Ultrasound (FUS) foundation and National Institutes of Health (NIH) (R01CA122276, R01CA111981).

REFERENCES

[1.] P. Wust, B. Hildebrandt, G. Sreenivasa, B. Rau, J. Gellermann, H. Riess, R. Felix and P. Schlag, "Hyperthermia in combined treatment of cancer," The lancet oncology, **3**, 487-497 (2002).

[2.] J. Van der Zee, "Heating the patient: a promising approach?," Annals of oncology, **13**, 1173-1184 (2002).

[3.] E. L. Jones, J. R. Oleson, L. R. Prosnitz, T. V. Samulski, Z. Vujaskovic, D. Yu, L. L. Sanders and M. W. Dewhirst, "Randomized trial of hyperthermia and radiation for superficial tumors," Journal of Clinical Oncology, **23**, 3079-3085 (2005).

[4.] Z. Vujaskovic, D. W. Kim, E. Jones, L. Lan, L. Mccall, M. W. Dewhirst, O. Craciunescu, P. Stauffer, V. Liotcheva and A. Betof, "A phase I/II study of neoadjuvant liposomal doxorubicin, paclitaxel, and hyperthermia in locally advanced breast cancer," International Journal of Hyperthermia, **26**, 514-521 (2010).

[5.] T. M. Zagar, J. R. Oleson, Z. Vujaskovic, M. W. Dewhirst, O. I. Craciunescu, K. L. Blackwell, L. R. Prosnitz and E. L. Jones, "Hyperthermia combined with radiation therapy for superficial breast cancer and chest wall recurrence: A review of the randomised data," International Journal of Hyperthermia, **26**, 612-617 (2010).

[6.] R. D. Issels, L. H. Lindner, J. Verweij, P. Wust, P. Reichardt, B.-C. Schem, S. Abdel-Rahman, S. Daugaard, C. Salat and C.-M. Wendtner, "Neo-adjuvant chemotherapy alone or with regional hyperthermia for localised high-risk soft-tissue sarcoma: a randomised phase 3 multicentre study," The lancet oncology, **11**, 561-570 (2010).

[7.] B. Hildebrandt, P. Wust, O. Ahlers, A. Dieing, G. Sreenivasa, T. Kerner, R. Felix and H. Riess, "The cellular and molecular basis of hyperthermia," Critical reviews in oncology/hematology, **43**, 33-56 (2002).

[8.] A. M. Ponce, Z. Vujaskovic, F. Yuan, D. Needham and M. W. Dewhirst, "Hyperthermia mediated liposomal drug delivery," International Journal of Hyperthermia, **22**, 205-213 (2006).

[9.] F. Lohr, K. Hu, Q. Huang, L. Zhang, T. V. Samulski, M. W. Dewhirst and C.-Y. Li, "Enhancement of radiotherapy by hyperthermia-regulated gene therapy," International Journal of Radiation Oncology Biology Physics, **48**, 1513-1518 (2000).

[10.] J. Lagendijk, "Hyperthermia treatment planning," Physics in medicine and biology, **45**, R61 (2000).

[11.] T. P. Ryan, "Comparison of six microwave antennas for hyperthermia treatment of cancer: SAR results for single antennas and arrays," International Journal of Radiation Oncology Biology Physics, **21**, 403-413 (1991).

[12.] C. J. Diederich and K. Hynynen, "Ultrasound technology for hyperthermia," Ultrasound in medicine & biology, **25**, 871-887 (1999).

[13.] M. Seegenschmiedt, L. Brady and R. Sauer, "Interstitial thermoradiotherapy: review on technical and clinical aspects," Am J Clin Oncol, **13**, 352-363 (1990).

[14.] J. H. Wootton, P. Prakash, I. C. J. Hsu and C. J. Diederich, "Implant strategies for endocervical and interstitial ultrasound hyperthermia adjunct to HDR brachytherapy for the treatment of cervical cancer," Physics in medicine and biology, **56**, 3967 (2011).

[15.] J. Crezee, P. Van Haaren, H. Westendorp, M. De Greef, H. Kok, J. Wiersma, G. Van Stam, J. Sijbrands, P. Zum Varde Sive Varding and J. Van Dijk, "Improving locoregional hyperthermia delivery using the 3-D controlled AMC-8 phased array hyperthermia system: A preclinical study," International Journal of Hyperthermia, **25**, 581-592 (2009).

[16.] K. A. Leopold, M. W. Dewhirst, T. V. Samulski, R. K. Dodge, S. L. George, J. L. Blivin, L. R. Prosnitz and J. R. Oleson, "Cumulative minutes with T_{90} greater than $temp_{index}$ is predictive of

response of superficial malignancies to hyperthermia and radiation," International Journal of Radiation Oncology Biology Physics, **25**, 841-847 (1993).

[17.] M. Franckena, D. Fatehi, M. Bruijne, R. A. M. Canters, Y. Norden, J. W. Mens, G. C. Rhoon and J. Zee, "Hyperthermia dose-effect relationship in 420 patients with cervical cancer treated with combined radiotherapy and hyperthermia," European Journal of Cancer, **45**, 1969-1978 (2009).

[18.] C. J. Diederich, J. Wootton, P. Prakash, V. Salgaonkar, T. Juang, S. Scott, X. Chen, A. Cunha, J. Pouliot and I. Hsu, "Catheter-based ultrasound hyperthermia with HDR brachytherapy for treatment of locally advanced cancer of the prostate and cervix," SPIE BiOS, 79010O-79010O-79018 (2011).

[19.] D. Needham and M. W. Dewhirst, "The development and testing of a new temperature-sensitive drug delivery system for the treatment of solid tumors," Advanced drug delivery reviews, **53**, 285-305 (2001).

[20.] P. Wust, C. H. Cho, B. Hildebrandt and J. Gellermann, "Thermal monitoring: Invasive, minimal-invasive and non-invasive approaches," International Journal of Hyperthermia, **22**, 255-262 (2006).

[21.] C. J. Diederich and K. Hynynen, "The development of intracavitary ultrasonic applicators for hyperthermia: A design and experimental study," Medical physics, **17**, 626 (1990).

[22.] C. Diederich and K. Hynynen, "The feasibility of using electrically focused ultrasound arrays to induce deep hyperthermia via body cavities," Ultrasonics, Ferroelectrics and Frequency Control, IEEE Transactions on, **38**, 207-219 (1991).

[23.] M. T. Buchanan and K. Hynynen, "Design and experimental evaluation of an intracavitary ultrasound phased array system for hyperthermia," Biomedical Engineering, IEEE Transactions on, **41**, 1178-1187 (1994).

[24.] L. Gavrilov and J. Hand, "Development and investigation of ultrasound linear phased arrays for transrectal treatment of prostate," Ultrasonics Sonochemistry, **4**, 173-174 (1997).

[25.] E. Hutchinson, M. Dahleh and K. Hynynen, "The feasibility of MRI feedback control for intracavitary phased array hyperthermia treatments," International Journal of Hyperthermia, **14**, 39-56 (1998).

[26.] N. B. Smith, M. T. Buchanan and K. Hynynen, "Transrectal ultrasound applicator for prostate heating monitored using MRI thermometry," International Journal of Radiation Oncology Biology Physics, **43**, 217-225 (1999).

[27.] M. Hurwitz, I. Kaplan, G. Svensson, M. Hansen and K. Hynynen, "Feasibility and patient tolerance of a novel transrectal ultrasound hyperthermia system for treatment of prostate cancer," International Journal of Hyperthermia, **17**, 31-37 (2001).

[28.] H. Fosmire, K. Hynynen, G. W. Drach, B. Stea, P. Swift and J. R. Cassady, "Feasibility and toxicity of transrectal ultrasound hyperthermia in the treatment of locally advanced adenocarcinoma of the prostate," International Journal of Radiation Oncology* Biology* Physics, **26**, 253-259 (1993).

[29.] M. D. Hurwitz, I. D. Kaplan, J. L. Hansen, S. Prokopios-Davos, G. P. Topulos, K. Wishnow, J. Manola, B. A. Bornstein and K. Hynynen, "Hyperthermia combined with radiation in treatment of locally advanced prostate cancer is associated with a favourable toxicity profile," International Journal of Hyperthermia, **21**, 649-656 (2005).

[30] M. D. Hurwitz, J. L. Hansen, S. Prokopiosa Davos, J. M
Hynynen and I. D. Kaplan, "Hyperthermia combined with radiation for the treatment of locally advanced prostate cancer," Cancer, **117**, 510-516 (2011).

[31] F. A. Jolesz, K. Hynynen, N. McDannold and C. Tempany, "MR imaging-controlled focused ultrasound ablation: a noninvasive image-guided surgery.," Magnetic resonance imaging clinics of North America, **13**, 545 (2005).

[32] C. M. Tempany, N. J. McDannold, K. Hynynen and F. A. Jolesz, "Focused ultrasound surgery in oncology: overview and principles," Radiology, **259**, 39-56 (2011).

[33] F. A. Jolesz, "MRI-guided focused ultrasound surgery," Annual review of medicine, **60**, 417-430 (2009).

[34] A. Partanen, M. Tillander, P. S. Yarmolenko, B. J. Wood, M. R. Dreher and M. O. Kahler, "Reduction of peak acoustic pressure and shaping of heated region by use of multifoci sonications in MR-guided high-intensity focused ultrasound mediated mild hyperthermia," Medical physics, **40**, 013301 (2013).

[35] Z. Mu, C. Ma, X. Chen, D. Cvetkovic, A. Pollack and L. Chen, "MR-guided pulsed high intensity focused ultrasound enhancement of docetaxel combined with radiotherapy for prostate cancer treatment," Physics in medicine and biology, **57**, 535 (2012).

[36] L. Chen, Z. Mu, P. Hachem, C. Ma, A. Wallentine and A. Pollack, "MR-guided focused ultrasound: enhancement of intratumoral uptake of [3H]-docetaxel in vivo," Physics in medicine and biology, **55**, 7399 (2010).

[37] X. Chen, D. Cvetkovic, C.-M. Ma and L. Chen, "Quantitative study of focused ultrasound enhanced doxorubicin delivery to prostate tumor in vivo with MRI guidance," Medical physics, **39**, 2780 (2012).

[38.] R. Staruch, R. Chopra and K. Hynynen, "Localised drug release using MRI-controlled focused ultrasound hyperthermia," International Journal of Hyperthermia, **27**, 156-171 (2010).

[39.] A. Partanen, P. S. Yarmolenko, A. Viitala, S. Appanaboyina, D. Haemmerich, A. Ranjan, G. Jacobs, D. Woods, J. Enholm and B. J. Wood, "Mild hyperthermia with magnetic resonance-guided high-intensity focused ultrasound for applications in drug delivery," International Journal of Hyperthermia, **28**, 320-336 (2012).

[40.] A. Napoli, M. Anzidei, C. De Nunzio, G. Cartocci, V. Panebianco, C. De Dominicis, C. Catalano, F. Petrucci and C. Leonardo, "Real-time Magnetic Resonance guided High-intensity Focused Ultrasound Focal Therapy for Localised Prostate Cancer: Preliminary Experience," European urology, (2012).

[41.] U. Lindner, S. Ghai, P. Spensieri, E. Hlasny, T. H. Van der Kwast, S. A. McCluskey, M. A. Haider, W. Kucharczyk and J. Trachtenberg, "Focal magnetic resonance guided focused ultrasound for prostate cancer: Initial North American experience," Canadian Urological Association Journal, **6**, E283 (2012).

[42.] FUSFoundation, "InSightec provides update on its prostate cancer clinical trial," http://www.fusfoundation.org/Focused-Ultrasound-Technology-News/insightec-provides-update-on-its-prostate-cancer-clinical-trial,

[43.] K. B. Ocheltree and L. Frizzel, "Sound field calculation for rectangular sources," Ultrasonics, Ferroelectrics and Frequency Control, IEEE Transactions on, **36**, 242-248 (1989).

[44.] J. H. Wootton, A. B. Ross and C. J. Diederich, "Prostate thermal therapy with high intensity transurethral ultrasound: The impact of pelvic bone heating on treatment delivery," International Journal of Hyperthermia, **23**, 609-622 (2007).

[45] H. H. Pennes, "Analysis of tissue and arterial blood temperatures in the resting human forearm," Journal of applied physiology, **1**, 93-122 (1948).

[46] B. O'Neill, C. Karmonik and K. Li, "An optimum method for pulsed high intensity focused ultrasound treatment of large volumes using the InSightec ExAblateÂ® 2000 system," Physics in medicine and biology, **55**, 6395 (2010).

[47] V. Rieke and K. Butts Pauly, "MR thermometry," Journal of Magnetic Resonance Imaging, **27**, 376-390 (2008).

[48] B. D. de Senneville, S. b. Roujol, C. Moonen and M. Ries, "Motion correction in MR thermometry of abdominal organs: a comparison of the referenceless vs. the multibaseline approach," Magnetic Resonance in Medicine, **64**, 1373-1381 (2010).

[49] B. Quesson, C. Laurent, G. Maclair, B. D. de Senneville, C. Mougenot, M. Ries, T. Carteret, A. Rullier and C. T. Moonen, "Real time volume ablation in vivo: a feasibility study in pig liver and kidney," NMR in Biomedicine, **24**, 145-153 (2011).

[50] M. D. Hurwitz, "Today's thermal therapy: not your father's hyperthermia: challenges and opportunities in application of hyperthermia for the 21st century cancer patient," American journal of clinical oncology, **33**, 96 (2010).

[51] B. Stawarz, H. Zielinski, S. Szmigielski, E. Rappaport, P. Debicki and Z. Petrovich, "Transrectal hyperthermia as palliative treatment for advanced adenocarcinoma of prostate and studies of cell-mediated immunity," Urology, **41**, 548-553 (1993).

[52] B. Frey, E.-M. Weiss, Y. Rubner, R. Wunderlich, O. J. Ott, R. Sauer, R. Fietkau and U. S. Gaipl, "Old and new facts about hyperthermia-induced modulations of the immune system," International Journal of Hyperthermia, **28**, 528-542 (2012).

[53] N. G. Choi, S. H. Soh, T. H. Yoon and M. H. Song, "Clinical experience with transurethral microwave thermotherapy for chronic nonbacterial prostatitis and prostatodynia," Journal of endourology, **8**, 61-64 (1994).

[54] M. Gao, H. Ding, G. Zhong, J. Lu, H. Wang, Q. Li and Z. Wang, "The Effects of Transrectal Radiofrequency Hyperthermia on Patients With Chronic Prostatitis and the Changes of MDA, NO, SOD, and Zn Levels in Pretreatment and Posttreatment," Urology, **79**, 391-396 (2012).

[55] E. S. Ebbini and C. A. Cain, "Multiple-focus ultrasound phased-array pattern synthesis: optimal driving-signal distributions for hyperthermia," Ultrasonics, Ferroelectrics and Frequency Control, IEEE Transactions on, **36**, 540-548 (1989).

[56] R. J. McGough, E. S. Ebbini and C. A. Cain, "Direct computation of ultrasound phased-array driving signals from a specified temperature distribution for hyperthermia," Biomedical Engineering, IEEE Transactions on, **39**, 825-835 (1992).

[57] D. Daum and K. Hynynen, "Theoretical design of a spherically sectioned phased array for ultrasound surgery of the liver," European journal of ultrasound, **9**, 61-69 (1999).

[58] B. Raaymakers, M. Van Vulpen, J. Lagendijk, A. De Leeuw, J. Crezee and J. Battermann, "Determination and validation of the actual 3D temperature distribution during interstitial hyperthermia of prostate carcinoma," Physics in medicine and biology, **46**, 3115 (2001).

[59] S. Goss, R. Johnston and F. Dunn, "Comprehensive compilation of empirical ultrasonic properties of mammalian tissues.," The Journal of the Acoustical Society of America, **64**, 423 (1978).

[60] K. Hynynen and D. DeYoung, "Temperature elevation at muscle-bone interface during scanned, focused ultrasound hyperthermia," International Journal of Hyperthermia, **4**, 267-279 (1988).

690

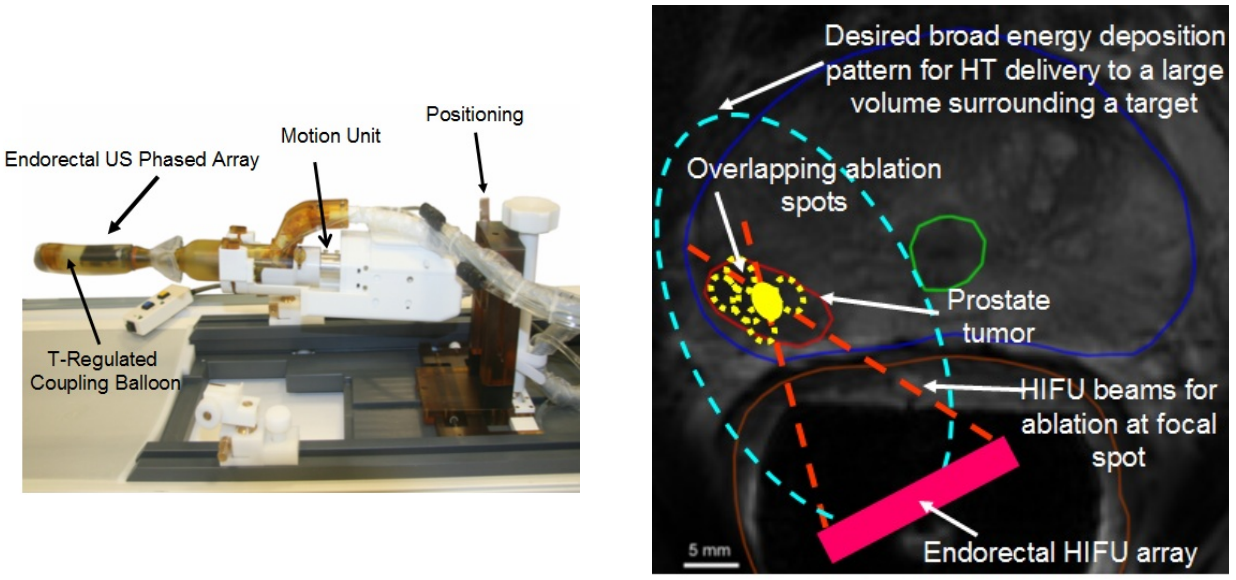

(a) (b)

Figure 1: (a) MR-compatible ExAblate 2100 endorectal ultrasound phased array (2.3 MHz) ablation system. (b) Illustration showing differences in sonications patterns required for ablation
695 and mild hyperthermia in the prostate to treat focal cancer lesions. The axial MR scan belongs to the representative patient case number 1 utilized during patient specific models presented in this paper.

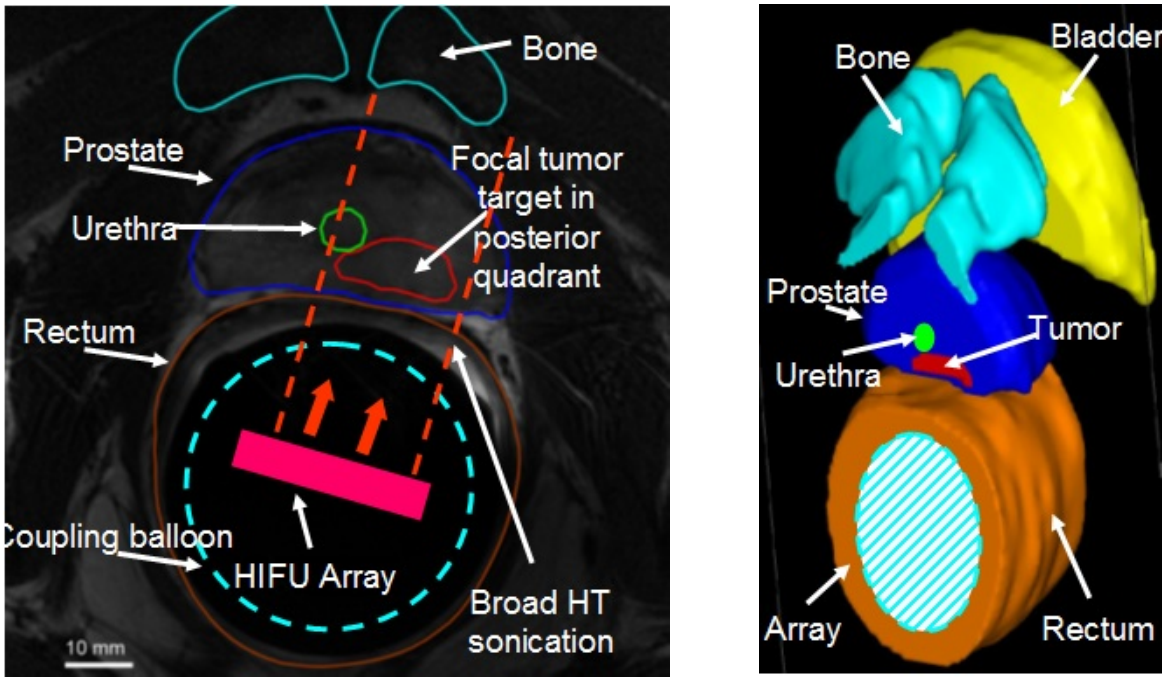

(a) (b)

Figure 2: (a) Axial MRI scan of with tumor target in prostate identified and segmented along with other critical anatomical structures. It belongs to the representative patient case number 2 utilized during patient specific models presented in this paper. (b) 3D model geometry created from serial axial scans following segmentation of organs.

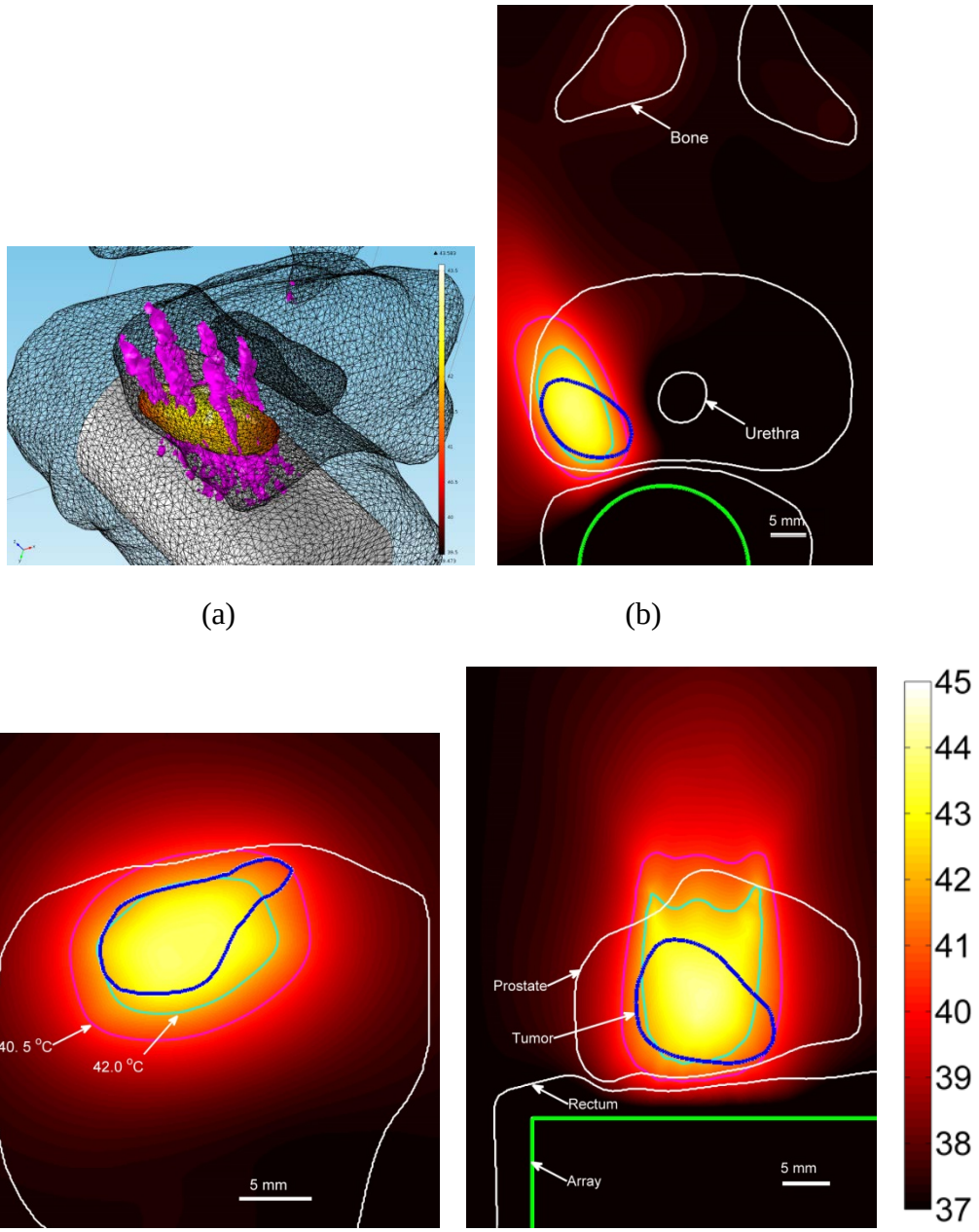

Figure 3: Conformable hyperthermia to a small focal region in the right quadrant of the prostate containing cancerous tissue. (a) Multi-focal pattern (six simultaneous foci) employed in hyperthermia delivery (plotted SAR contour = 300 W/kg) is overlaid upon 3D anatomical geometry along with temperature on tumor surface. Temperature distribution plotted in (b) axial, (c) coronal and (d) sagittal planes through target center ($I = 3.4$ W/cm^2, $T_{max} = 44.9$ ^oC).

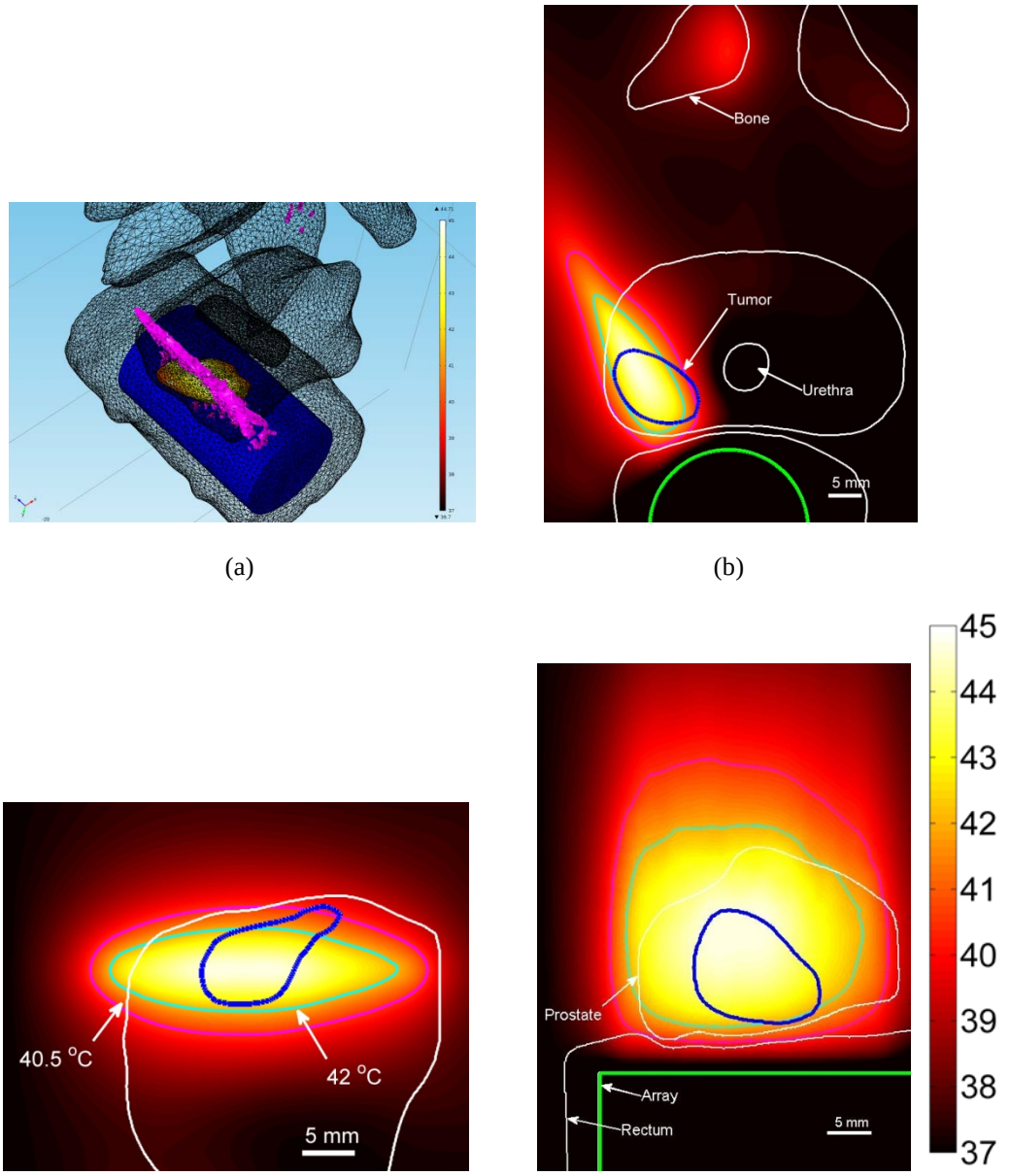

(a) (b)

(c) (d)

Figure 4: Hyperthermia to a small focal cancer target region in right quadrant of the prostate using curvilinear focusing. (a) Curvilinear focusing (35 mm depth) pattern (plotted SAR contour = 300 W/kg) is overlaid upon 3D anatomical geometry, along with temperature on tumor surface. Temperature distribution plotted in (b) axial, (c) coronal and (d) sagittal planes through tumor center ($I = 0.75$ W/cm^2, $T_{max} = 44.7$ ^{o}C).

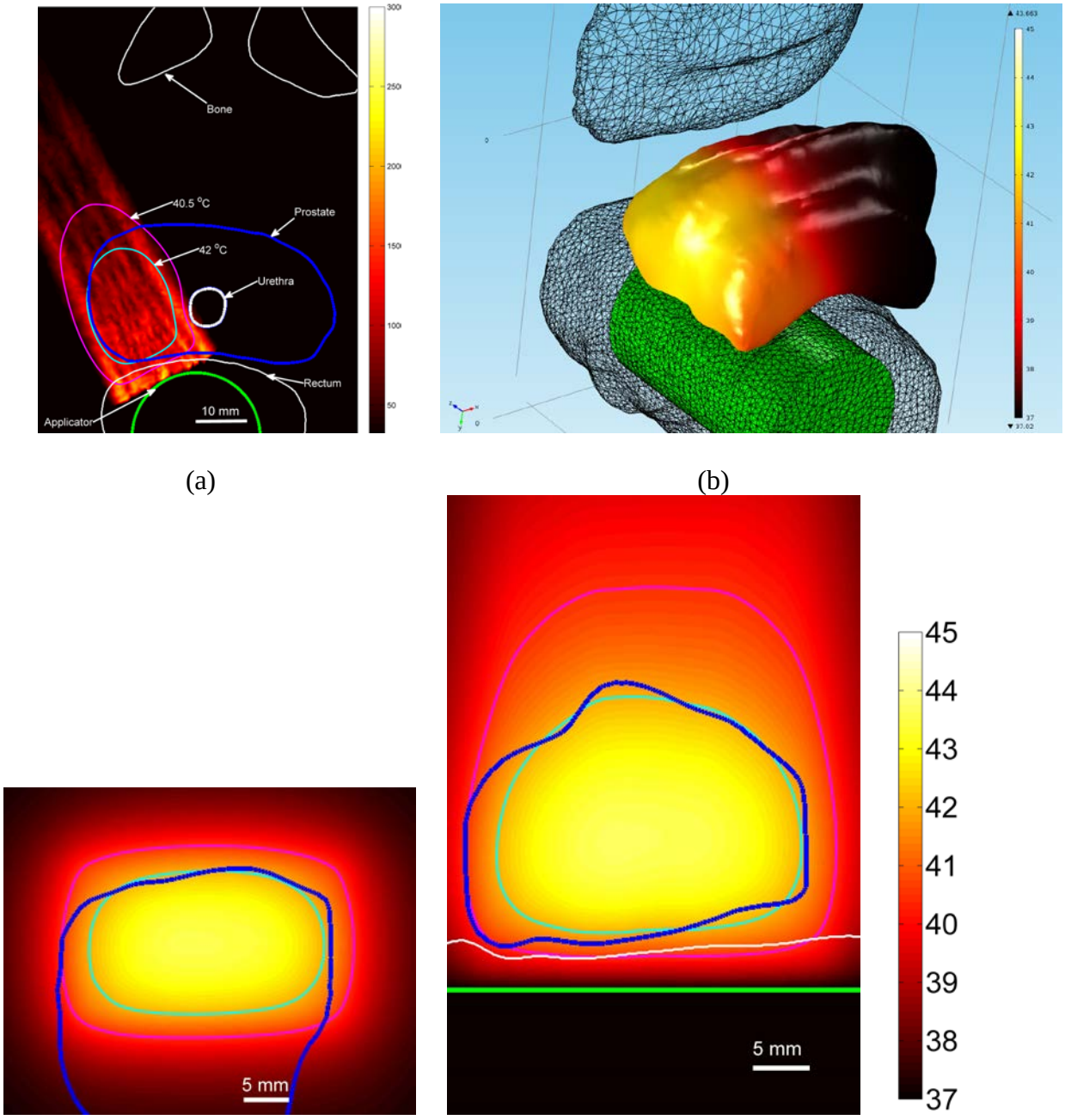

Figure 5: (a) SAR distribution obtained by planar sonication is plotted in the central axial plane of a representative case. Temperature and anatomy overlay to show hemi-gland heating of the prostate is shown in (b) 3D, (c) coronal plane 30 mm from the applicator and (d) sagittal plane through the applicator. Applicator is shown in green, prostate is shown in blue ($I = 0.9$ W/cm^2, $T_{max} = 43.7$ ^{o}C).

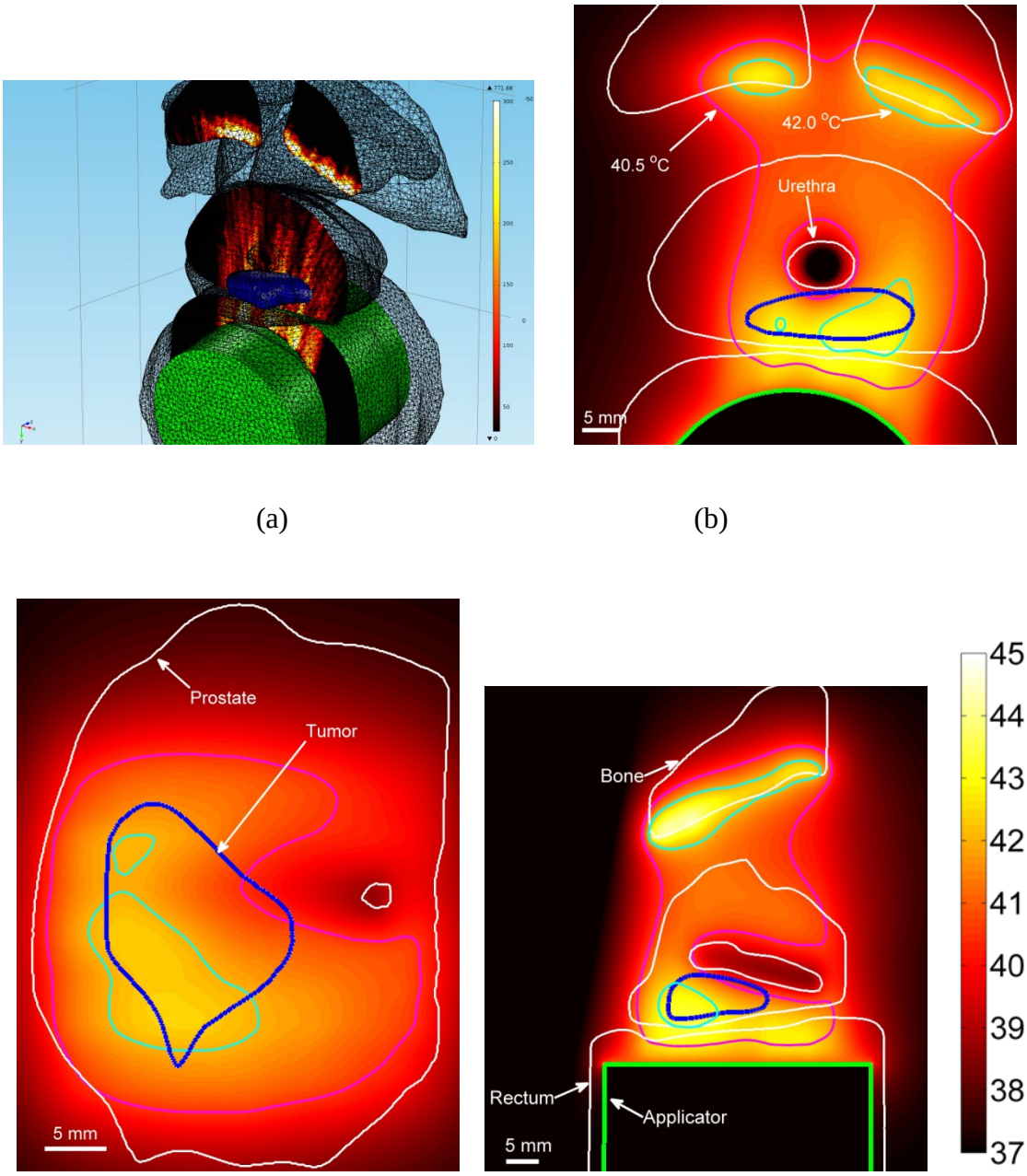

(a) (b)

(c) (d)

Figure 6: (a) SAR distribution obtained by cylindrically diverging sonication is plotted in the central axial plane (b) Corresponding temperature distribution obtained in the same central axial plane is shown. Temperature distribution in an oblique sagittal slice (c) and an oblique coronal slice is also shown. For all sub-plots, tumor contour is shown in blue, organs are shown in white and applicator placement is shown in green ($I = 1.35$ W/cm^2, $T_{max} = 44.8$ ^{o}C).

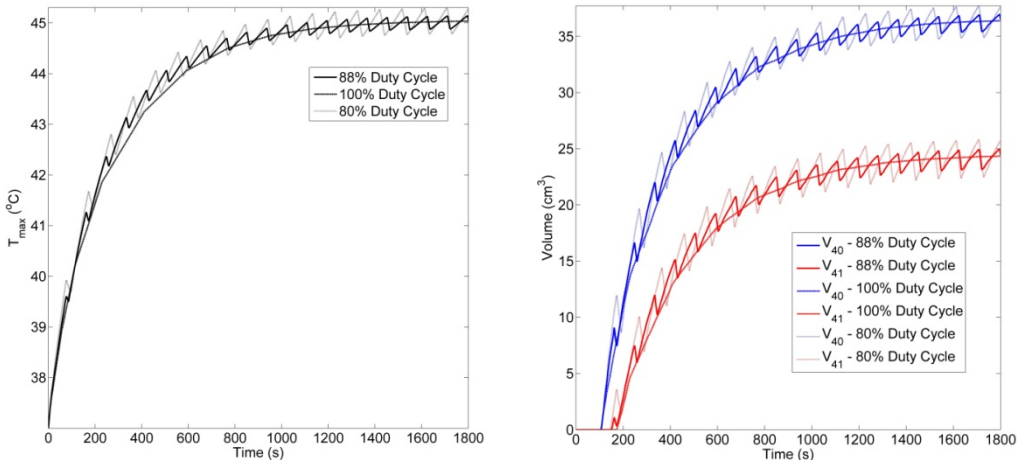

(a) (b)

Figure 7: Comparison of (a) T_{max} *vs*. time, (b) V_{40}, V_{41} *vs*. time for 80%, 88% and 100% duty cycle for planar sonication in generalized model is shown here. Acoustic intensity was adjusted to maintain constant energy.

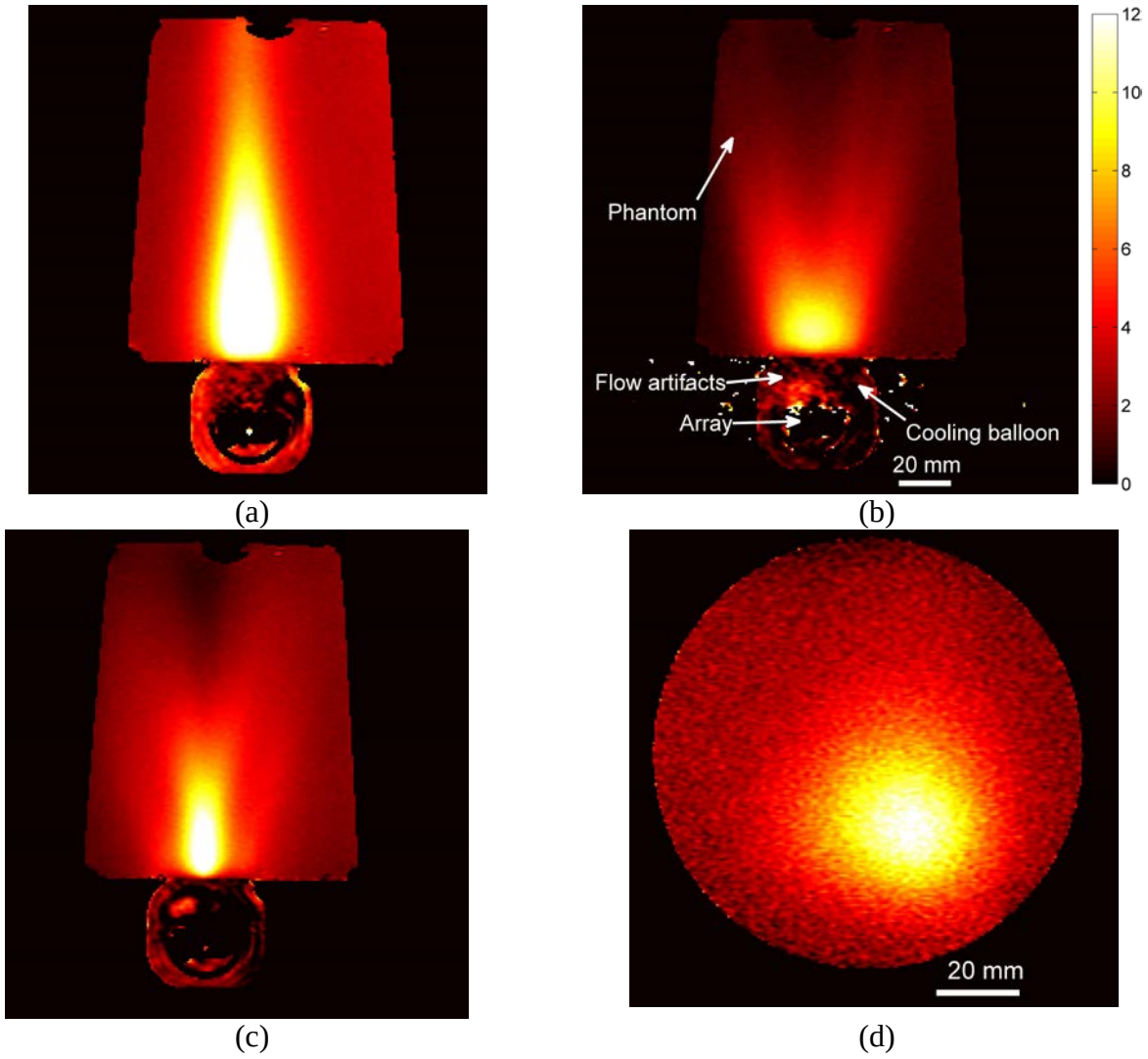

Figure 8: MR temperature images captured during CW sonications in tissue mimicking phantoms with ExAblate 2100 prostate array are shown here (0.86 W/cm2, 15 min.). Heating from (a) Iso-phase/planar, (b) diverging and (c) curvilinear in axial plane and (d) simultaneous multi-focused sonications in coronal plane are shown.

Parameter	Units	Value
k (thermal conductivity)	W/m/^{o}C	0.56
ω_b (blood perfusion)	kg/m^3/s	0.5 – 8.0 (Range used in generalized model) 1 (bone) 2.5 (prostate) 5 (peri-prostatic tissue) 4 (rectum)
C_b (specific heat of blood)	J/kg/^{o}C	3720
C (specific heat of tissue)	J/kg/^{o}C	3600
T_b (body/blood temperature)	^{o}C	37
c (sound speed)	m/s	1500
ρ (density)	Kg/m^3	1060
f_0 (center frequency)	MHz	2.3
α (acoustic absorption), μ (acoustic attenuation)	Np/m/MHz	5.3 (Generalized model) 5.3 (prostate) 6 (rectum) 5 (peri-prostatic tissue) 250 (bone)

Table 1: Constants used in biothermal and acoustic models are tabulated here. These values have been obtained from Refs. (44, 58-60). Physical and physiological properties of tissue were assumed to be homogeneous in generalized models, and varied with tissue type in patient-specific models.

Number	Is (W/cm^2)	T_{max} (^oC)	V_{40} (cm^3)	V_{41} (cm^3)
4	2	44.6	5.5	2.7
6	3.4	44.7	7.2	3.9
8	3.4	42.3	3.8	1.5

Table 2: Treatable volumes obtained by multi-point focusing in generalized models. The number of simultaneous focusing points was varied. Power input was adjusted to achieve maximum temperature close to 45 ^oC, within limits and constraints necessary for safe operation on ExAblate 2100. Constant blood perfusion of 2 $kg/m^3/s$ was assumed.

Depth (mm)	Is (W/cm^2)	T_{max} (^oC)	V_{40} (cm^3)	V_{41} (cm^3)
25	0.75	45.1	12.1	6.0
35	0.7	44.9	12.7	6.6

Table 3: Treatable volumes obtained by cylindrical or curvilinear focusing in generalized models. The focal depth was varied. Power input was adjusted to achieve maximum temperature close to 45 ^oC, within limits and constraints necessary for safe operation on ExAblate 2100. Constant blood perfusion of 2 $kg/m^3/s$ was assumed.

Pos. (mm)	Is (W/cm^2)	T_{max} (^oC)	V_{40} (cm^3)	V_{41} (cm^3)
10	1.05	44.7	24.4	13.3
20	1.13	44.7	26.3	13.8
40	1.2	44.8	37.2	21.5

785 Table 4: Treatable volumes obtained by divergent focusing in generalized models. The divergence angle was varied. Power input was adjusted to achieve maximum temperature close to 45 ^oC, within limits and constraints necessary for safe operation on ExAblate 2100. Constant blood perfusion of 2 $kg/m^3/s$ was assumed.

Type	Is (W/cm^2)	T_{max} (^oC)	V_{40} (cm^3)	V_{41} (cm^3)
Planar	0.94	44.7	35	22.8

Table 5: Treatable volumes obtained by planar or iso-phase focusing in generalized models. Power input was adjusted to achieve maximum temperature close to 45 ^oC, within limits and constraints necessary for safe operation on ExAblate 2100. Constant blood perfusion of 2 $kg/m^3/s$ was assumed.

			40 °C contour dimensions				41 °C contour dimensions			
ω_b	I	T_{max}	Azim	Elev	Range	Spare	Azim	Elev	Range	Spare
(kg/m^3/s)	(W/cm^2)	(°C)	(mm)	(mm)	(mm)	(mm)	(mm)	(mm)	(mm)	(mm)
0.5	0.61	45.02	33	40	71.5	21.5	27	35	67	23
2.0	0.99	45.06	29	38	71	20	24	34	65	21
4.0	1.43	44.98	26	37	70	19	23	34	62.5	20
8.0	2.15	44.96	26	37	69	17.5	22	33	59	18.5

Table 6: Parametric study was conducted using planar sonication implemented in steady state generalized models to study the impact of perfusion on heat delivery. The perfusion was varied between 0.5 – 8.0 kg/m^3/s. Acoustic intensity was varied such that the maximum temperature was close to 45 °C. Dimensions of 40 °C and 41 °C contours are reported here. Azim refers to dimension along transducer width, Elev refers to the dimension along array length, Range refers to axial depth from transducer surface, and Spare refers to distance of tissue from cooling/coupling balloon which was thermally spared (not heated above 40 °C or 41 °C). Cooling around the device was held constant and the balloon was modeled as a constant temperature boundary at 30 °C.

			40 ^{o}C contour dimensions				41 ^{o}C contour dimensions			
T_c	I	T_{max}	Azim	Elev	Range	Spare	Azim	Elev	Range	Spare
(^{o}C)	(W/cm^2)	(^{o}C)	(mm)	(mm)	(mm)	(mm)	(mm)	(mm)	(mm)	(mm)
22	1.05	45.01	28	38	71.5	22.5	24	34	66.5	23.5
30	0.99	45.06	29	38	71	20	24	34	65	21
35	0.92	44.94	28	38	69.5	17.5	24	34	63	19

Table 7: Parametric study was conducted using planar sonication implemented in steady state generalized models to study the impact of applicator cooling on heat delivery. Cooling was varied from 22 – 35 ^{o}C. The perfusion was set to 2.0 kg/m^3/s. Acoustic intensity was varied such that the maximum temperature was close to 45 ^{o}C. Dimensions of 40 ^{o}C and 41 ^{o}C contours are reported here. Azim, Elev, Range and Spare are same as in previous table.

			t_{43} > 6 min contour dimensions				t_{43} > 10 min contour dimensions			
Duty Cyc.	*I*	T_{max}	Azim	Elev	Range	Spare	Azim	Elev	Range	Spare
(%)	(W/cm^2)	(^{o}C)	(mm)	(mm)	(mm)	(mm)	(mm)	(mm)	(mm)	(mm)
100	0.99	45.06	20	32	56	23	18.8	28	53	23
88	1.12	45.06	20	32	56	23	18	28	53	23
80	1.25	45.28	20	32	56	23	18	28	53	23

Table 8: Parametric study was conducted using planar sonication implemented in transient generalized models to study the impact of sonication duty cycle on heat delivery. Duty cycle was varied between 80%, 88% and 100% with pulse repetition frequency 0.0104 Hz, 0.011 Hz and CW. The perfusion was set to 2.0 kg/m^3/s and cooling temperature was held constant at 30 ^{o}C. Peak acoustic intensity was varied such that the total energy delivered in a single pulse cycle was constant and the maximum temperature was close to 45 ^{o}C. Dimensions of t_{43} > 6 min and t_{43} > 10 min contours are reported here. Azim, Elev, Range and Spare are same as in previous tables.

INSTITUTIONAL ANIMAL CARE AND USE COMMITTEE
Office of Research, Box 0547
University of California San Francisco

A P P R O V A L L E T T E R

December 13, 2012

Viola Rieke
Box 0946

APPROVAL NUMBER: AN088193-01

Approval Date: December 13, 2012
Expiration Date: December 13, 2013

Title: MR-guided cardiac focused ultrasound ablation

The IACUC approval number should be used for ordering animals and should be included in any correspondence regarding this study. This approval letter supersedes all previous approvals.

All individual participants must read the final approved protocol which must be followed exactly as written. Any modifications to this protocol must be submitted using the RIO online system. Modifications may not be implemented until reviewed and approved by the IACUC.

Non-compliance with any of these conditions violates federal and state laws and regulations, and University policies and guidelines governing the care and use of laboratory animals. Violations may have serious consequences for the welfare of your animals, your laboratory's ability to conduct animal research, and may impact funding from NIH.

UCSF requires health & safety review of all animal use protocols. Refer to OEH&S review letter for details. You may not work with hazardous materials in animals until OEH&S authorizations are current.

If you have questions, contact the IACUC Office at 476-2197 or email iacuc@ucsf.edu.

Animals Approved

Swine - USDA Type D, Acquired - 4

Personnel Approved

Rieke, Viola - Emergency Contact 1, Principal Investigator

Saeed, Maythem - Alternate Responsible, Emergency Contact 2

John Taylor, Ph.D.
Chair, Institutional Animal Care and Use Committee